



# A Review on Computational Methods for Denoising and Detecting ECG Signals to Detect Cardiovascular Diseases

Prashant Mani Tripathi<sup>1</sup> · Ashish Kumar<sup>2</sup> · Rama Komaragiri<sup>1</sup> · Manjeet Kumar<sup>3</sup>

Received: 25 May 2021 / Accepted: 30 August 2021 / Published online: 13 October 2021  
© CIMNE, Barcelona, Spain 2021

## Abstract

Cardiac health of the human heart is an intriguing issue for many decades as cardiovascular diseases (CVDs) are the leading cause of death worldwide. Electrocardiogram (ECG) signal is a powerful complete non-invasive tool for analyzing cardiac health. ECG signal is the primary choice of various health practitioners to determine vital information about the human heart. In the literature, the ECG signals are studied to diagnose and detect heart abnormalities such as enlargement of a heart chamber, detect cardiovascular diseases, detect ischemia, measure heart rate, biometric identification, and name a few. ECG signal being feeble suffers from the different kinds of noises, which might damage the ECG signal's morphological features, leading to wrong information and improper treatment. Removal of the noises from the ECG signal is an essential part of ECG signal processing. The denoised ECG signal facilitates the correct detection of the morphological features, which provides appropriate information about the cardiac health of the human heart. Detection of morphological features typically includes detecting QRS complex, R peak, and other ECG signal characteristics. These detected features are used to predict CVDs and other heart abnormalities. Earlier and accurate detection of CVDs involves two main steps: denoising and detection of a morphological feature. The increasing mortality rate due to CVDs compelled researchers to invent efficient computational techniques that automatically detect abnormalities in the heart. In the past few decades, various researchers have been proposed many computational methods to denoise and detect the ECG signal. This paper presents a comparative study of various existing state-of-the-art techniques used to analyze the ECG signal. Various noises influence the performance of the existing computational methods; hence, a summary of the different noises presented in the ECG signal is also included. The advantages and drawbacks of each method for ECG signal denoising and detection are discussed briefly. The efficiency of denoising and detection techniques was evaluated by testing the proposed algorithms using different standard databases like MIT-BIH, AHA, PTB, MIT-BIH noise stress test, Apnea-ECG. Details of these standard databases are provided in the paper. The performance of existing ECG signal denoising and detection algorithms is compared using parameters like signal-to-noise ratio improvement, percentage root mean square difference, root mean square error, sensitivity, positive predictivity, error, and accuracy. Finally, the challenges and gaps of the existing state-of-the-art techniques to analyze the ECG signal for automatic detection of CVDs are discussed.

✉ Manjeet Kumar  
manjeetchhillar@gmail.com

Prashant Mani Tripathi  
pmanitripathi@gmail.com

Ashish Kumar  
akumar.1june@gmail.com

Rama Komaragiri  
rama.komaragiri@gmail.com

<sup>1</sup> Department of Electronics and Communication Engineering, Bennett University, Greater Noida, India

<sup>2</sup> School of Electronics Engineering, Vellore Institute of Technology, Chennai, Tamil Nadu, India

<sup>3</sup> Department of Electronics and Communication Engineering, Delhi Technological University, Delhi, India

## 1 Introduction

Cardiovascular diseases (CVDs) are a major health concern to humanity. The mortality rate due to CVDs is still the highest across the world. In 2016, as per the World Health Organization (WHO) report, 17.9 million died due to cardiovascular diseases. Out of these, 85% of deaths are because of stroke and heart attack. In low and middle-income countries, the number of deaths caused by CVDs is huge [1]. Economically, CVDs are leaving an enormous burden on societal resources. Increasing stress due to lifestyle changes, hypertension, unhealthy diet, obesity, physical inactivity, diabetes, hyperlipidemia, consumption of harmful

substances like tobacco and alcohol can cause cardiovascular diseases. Major cardiovascular diseases include congenital heart defects, coronary artery disease, cardiomyopathy, myocarditis, and myocardial infarction [2]. Early detection and diagnosis are vital to prevent and treat cardiovascular diseases. Real-time monitoring of heart activity is required to detect CVDs accurately. Electrocardiogram (ECG), echocardiogram, cardiac catheterization, cardiac computerized tomography scan, and cardiac magnetic resonance imaging are some popular methods to detect CVDs. ECG depicts a graphic pattern that represents the electrical and muscular function of the heart. Being a non-invasive method, ECG avoids the perils of invasive methods. ECG measured from the skin of a subject provides the electrical activity of different cardiac tissues within the heart and is shown in Fig. 1. ECG is a reliable, popular, inexpensive method to trace and study the electrical activity of a heart, hence making it ubiquitous. A careful analysis of each heartbeat is required to detect CVDs [3, 4].

Nowadays, ECG is not only used to detect CVDs but also used for various other purposes like biometric identification [6], identification of various other diseases like pneumonia [7], estimation of respiratory frequency [8]. The ECG waveform mainly consists of *P*, *Q*, *R*, *S*, and *T* waves, as shown in Fig. 2. A detailed description of an ECG waveform is found in [9]. The detailed description of amplitude, frequency, duration, and origin is summarized in Table 1 [5, 10–12]. The amplitude values in Table 1 are measured across lead II. The wave amplitude is measured with reference to the ECG signal baseline level defined by the isoelectric line, immediately preceding the QRS complex. Two-time instants determine the duration of a wave; the wave either crosses the baseline or deviates significantly from the zero reference line [5]. As the researchers use ECG for cardiac monitoring and

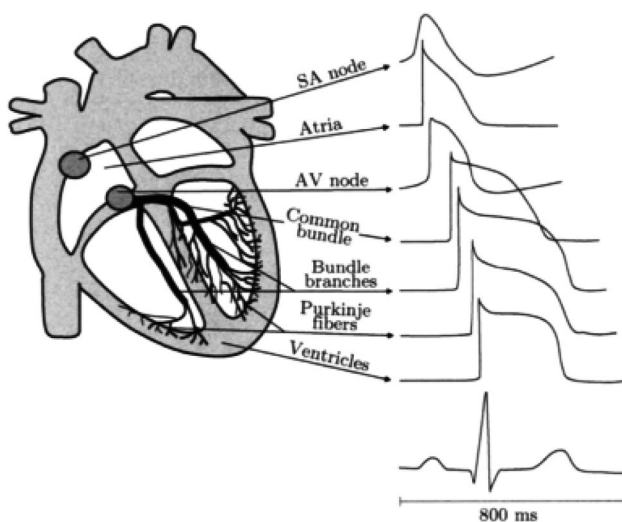


Fig. 1 The electrical activity of various cardiac tissues [5]

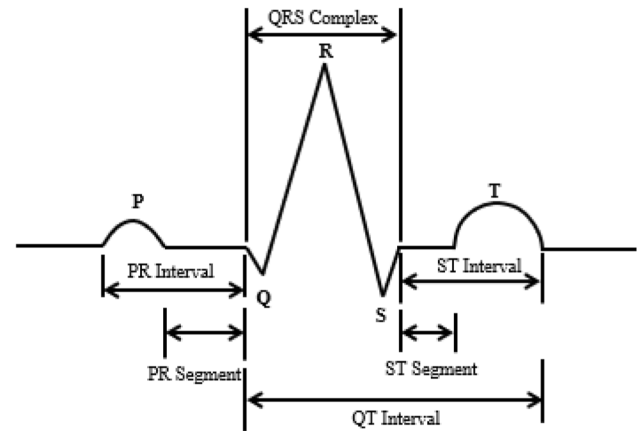


Fig. 2 Basic ECG waveform

various applications, it is essential to analyze and classify the ECG signals sensibly and precisely. During continuous monitoring, manual analysis of an ECG signal is a tedious and erroneous task. Hence, an automatic system to analyze and classify the ECG signal is in great demand.

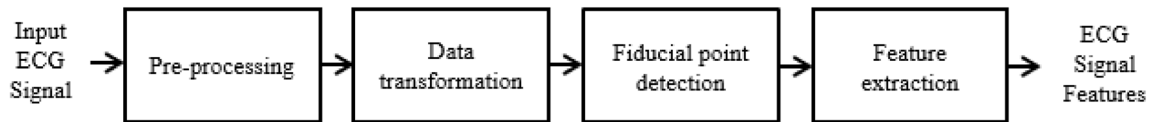
A fully automatic system to analyze and categorize an ECG signal includes various steps like pre-processing, data transformation, fiducial point detection, and feature extraction. The block diagram representing various steps involved in the ECG signal analysis are shown in Fig. 3. Pre-processing or noise filtering is vital because it directly influences the performance of the system. Hence removing various kinds of noise present in the ECG signal is vital and challenging.

The pre-processed signal is applied to data transformation, which includes processes like differentiation and squaring. The purpose of this data transformation is to compute the slope and width information of the QRS complex. The derivative stage provides the slope information of the QRS complex while squaring operation converts the bipolar signal into a unipolar signal and provides non-linear amplification to the output of the derivative stage. The squaring operation helps minimize the false positive caused by the T waves, whose energies are higher than usual spectral energies [13]. The moving window integration provides a signal which contains the slope and width information of the QRS complex [13]. This vital information (slope and width of the QRS complex) is used to detect the R peak (peak of QRS complex). The feature extraction unit extracts various statistical and morphological features of an ECG signal, including P-wave, QRS complex, and T wave. With the features mentioned above, the ECG signal is analyzed to obtain various heart conditions.

The organization of the paper is as follows. In Sect. 2, different types of noises are discussed. Pre-processing or denoising techniques are presented in Sect. 3. Section 4 includes data transformation and detection techniques.

**Table 1** Summary of various ECG waveform

Wave	Frequency	Origin	Amplitude	Duration
P	0.67–5 Hz	Depolarization of atrial musculature	0.25 mV	< 120 ms
Q	10–50 Hz	QRS complex reflects depolarization of the right and left ventricles	25% of R Wave	70–110 ms
R			1.60 mV	
S			–	
T	1–7 Hz	Ventricular repolarisation	0.1–0.5 mV	100–250 ms

**Fig. 3** ECG signal processing algorithm

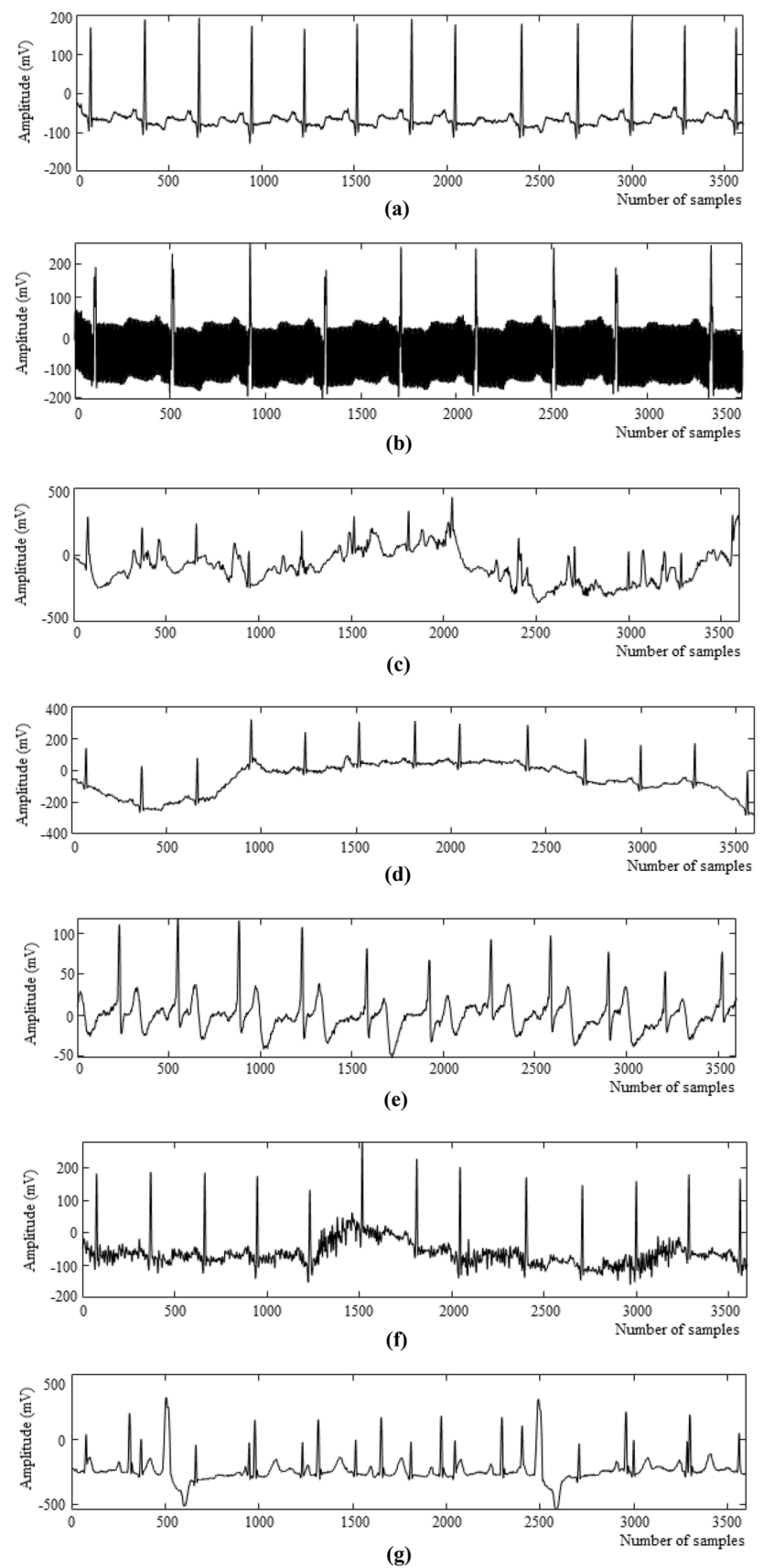
Various databases are discussed in Sect. 5. Evaluation parameters are introduced in Sect. 6. Section 7 includes discussion and challenges. Finally, conclusions are presented in Sect. 8.

## 2 Noises in ECG Signal

Noise, the most critical object in the ECG signal analysis, must be given full attention to accurately and precisely detect QRS complexes. Various noises present in an input ECG signal must be filtered before proceeding to further processing. Various noise and artifacts that contaminate an ECG signal are briefly discussed below.

- (a) *Power line Interference (PLI)* is the most common noise in the ECG signal is due to the inductive interference between the power line and the electronics of ECG recording equipment. PLI has an amplitude of up to 50% of peak-to-peak ECG amplitude. The frequency of PLI is 60 Hz and its harmonics (or  $50 \pm 0.2$  Hz in some data sets). Signal amplitude and frequency both vary with the power line interference. The bandwidth of this noise is below 1 Hz [14]. Figure 4a shows the reference ECG signal (record 100) taken from the MIT-BIH arrhythmia database, while the PLI included signal is shown in Fig. 4b.
- (b) *Electrode Contact Noise* is a randomly occurring noise with an amplitude equal to maximum recorder output. The loss of contact between skin and electrodes results in a transient interference with a one-second duration. The contact break can be permanent; it can be spasmodic when a loose electrode comes into contact or out of contact with the skin due to vibration and movement. The consequence of this noise is the baseline transition, which decreases exponentially to the base-
- line value [14]. The effect of electrode contact noise on MIT-BIH record 100 is shown in Fig. 4c.
- (c) *Baseline Wander or baseline shift* is a low-frequency noise in the frequency range of 0.15–0.3 Hz with an amplitude of 15% of peak-to-peak ECG amplitude. This noise arises from the respiration of the subject and forces the baseline shift in the ECG signal. Baseline wandering increases with an increased breathing rate. Various aspects like impedance of the skin, the subject's movement, electrode features, and electrolyte properties influence the baseline shift's amplitude and duration [15, 16]. Figure 4d represents the effect of baseline wander on MIT-BIH ECG record 100.
- (d) *Motion Artifacts* result from the electrode movement over the skin due to movements by the subject. The movement of electrodes causes a change in the skin–electrode impedance, resulting in a variation in the ECG signal baseline. The amplitude of motion artifact is about 500% of peak-to-peak ECG signal amplitude for a duration ranging from 100–500 ms. The motion artifact thus results in a transient baseline change. Motion artifacts and baseline wander can damage the low-frequency component and ST-segment of the ECG signal. Distorted ST-segment may lead to a false prediction of various diseases like myocarditis, ischemia, infarction, Brugada syndrome, infiltrative or myopathic processes [15, 16]. Motion artifacts are shown in Fig. 4e.
- (e) *Electromyographic (EMG)* noise is due to muscle contraction, which generates potentials in the millivolt range. The duration of EMG noise is 50 ms and contains frequency components in the range of 0–10 kHz. The average amplitude of EMG noise is about 10% of peak-to-peak ECG signal amplitude. The EMG noise overlaps with the ECG signal in the 0.01–0.1 kHz frequency range [15, 16]. Removal of this noise without

**Fig. 4** Effect of various noises on ECG signal, **a** MIT-BIH arrhythmia record 100 **b** powerline interference, **c** electrode contact noise, **d** baseline drift, **e** motion artefacts, **f** muscle contraction, **g** instrumentation noise



disturbing the features in an ECG signal is quite tricky. The effect of EMG noise on MIT-BIH ECG record 100 is represented in Fig. 4f.

- (f) *Instrumentation Noise* is produced by improper usage of electronic components used to record ECG signals. An example of instrumentation noise is the saturation in the amplitude of an ECG signal due to improper biasing of an input amplifier, thus causing an improper recording of ECG signal [15, 16]. Instrumentation noise is shown in Fig. 4g.
- (g) *Electrosurgical Noise* is the noise produced by the medical equipment present in the patient monitoring environment. This type of noise significantly corrupts the ECG signals. This noise is modeled as a sinusoidal of large amplitude with frequencies ranging between 0.1–1 MHz for 1–10 s. The amplitude of this noise is approximately 200% of peak-to-peak ECG amplitude.

### 3 Pre-processing of ECG Signal

Until the 1970s, the direct-writing electrocardiograph was prominent, and the recorded signals were analog. Before further processing, nearly all ECG machines digitize the analog ECG signal at a particular sampling rate [17] using analog to digital (A/D) conversion techniques. At the front end, the initial A/D conversion sampling rate is significantly higher than the targeted sampling rate of the ECG signal processing. This higher initial sampling rate is known as oversampling. Oversampling is required to detect the output stimulus of a pacemaker with a duration of smaller than 0.5 ms. Oversampling has other advantages like improvement in quantization error regarding the precision of the least significant bit and implementation of lower-order analog anti-aliasing filter [17, 18]. In the sampling process, aliasing is a common problem that must be removed. To remove aliasing, LPF is used, known as an anti-aliasing filter. In ECG signal processing, two LPFs are used to avoid aliasing: an analog LPF and a digital decimation LPF. The analog anti-aliasing LPF is used before A/D conversion for the oversampling process. Digital decimation LPF is located after digitization for the down-sampling process. If both the filters have weak attenuation at their stopbands, aliasing could appear [17].

The analog LPF at the front of an A/D converter avoids aliasing by limiting the spectrum of the input ECG signal at the limit set by the Nyquist criterion. The analog LPF performs three more functions: offer a flat frequency response in the passband, minimize non-linear phase response, and oversampling cut-off much higher than 150 Hz. Similarly, the decimation filter provides a flat frequency response in the passband and sets the upper cut-off frequency at 150 Hz with 3-dB attenuation [17]. However, the implementation of an analog filter involves low tolerance value resistors and

capacitors. When realized using VLSI implementation, their IC requires considerable chip area with the increased process and circuit complexity. The resistors implemented in VLSI circuits have a vast process variation. As the quality factor and resonant frequency of a filter depend on component values, the process variations result in huge circuit variations. The parasitic capacitances can also affect the performance of the circuits. Parasitic capacitances significantly affect high impedance nodes due to their small values [19].

Various noise removal techniques have been proposed to suppress noises and artifacts in an ECG signal in the last few decades. A detailed description of noise removal techniques is provided in Table 2. Filters are attractive tools for ECG signal pre-processing and denoising. Digital filters are preferred over analog filters to remove noises and artifacts [20, 21] as digital filter offers design flexibility. A digital filter can be implemented in a software environment before realizing it as hardware. Any change in filter characteristics can be realized in a digital filter by merely changing the filter coefficients, which is achieved by tweaking the program code. Once the performance is satisfactory, then the digital filter can be realized using hardware. Physical reconstruction of a circuit is required to design an analog filter that demands more time and cost to implement. Unlike analog filters, digital filters are immune to environmental conditions and the aging effect as their operation depends on numerical computations rather than the electrical characteristics of components [22]. The cutoff frequency of a digital filter can be represented with excellent precision, while in analog filtering, a 5% deviation in cutoff frequency is accepted [22, 23]. These virtues of the digital filter make them suitable for analyzing very low-frequency signals. Various researchers use various types of filters like a low-pass filter (LPF), high-pass filter (HPF), a band-pass filter (BPF), median, notch, adaptive, Savitsky-Golay (S-G), Moving average (MA) for noise removal.

LPF is a universally accepted method for ECG denoising [24]. The low-pass filter removes high-frequency components of an ECG waveform and leaves a significant portion of the ECG waveform for further processing. The popular cut-off frequencies of low-pass filters in ECG signal analysis are 11 Hz, 30 Hz, 35 Hz, 50 Hz, 90 Hz. A low-pass filter removes high-frequency noises like PLI, EMG but, more importantly, affects high-frequency components of ECG signals such as QRS complex, pacemaker spike and J-wave [62–64]. To preserve these useful high-frequency components, the American Heart Association (AHA) has changed its recommendation for cut-off frequencies of the low-pass filter from 35 to 150 Hz and 250 Hz for adults and children, respectively [17, 65]. The effect of LPF on an ECG record 203, taken from the MIT-BIH arrhythmia database, is shown in Fig. 5. Figure 5a represents the original MIT-BIH record 203 and the low-pass filtered version of this ECG record,

**Table 2** Overview of studies conducted on ECG signal denoising

References	Method	Database	Record	Evaluation parameters
Lee and Hwang, 2018 [24]	High-pass filter+low-pass filter+periodic non-local means filter	MIT-BIH	100, 103, 104, 105, 106, 115, and 215	$SNR_{IMP} = 7.678$ dB (avg.), $MSE \approx 0.0010$ , $PRD > 10\%$ (for 10 dB I/P SNR for white noise) $SNR_{IMP} = 3.987$ dB (avg.), $MSE > 0.0010$ , $PRD > 12\%$ (for 10 dB I/P SNR for pink noise) $SNR_{IMP} = 4.757$ dB (avg.), $MSE = 0.0020$ , $PRD > 15\%$ (for 10 dB I/P SNR EMG) No artifactual fluctuation
Wang et al., 2019 [25]	Linear time-invariant filtering + sparse optimization	MIT-BIH NSTDB	103, 105, and 213	$SNR_{out} = 15.94$ dB, $MSE = 0.003$ dB (5 dB I/P SNR for record 103)
Wang et al., 2015 [26]	Parallel-type fractional zero-phase filtering	MIT-BIH	115	$SNR = 14.2565$ dB, $MSE = 0.0128$ (50 Hz PLI) $SNR = 13.6817$ dB, $MSE = 0.0146$ (EMG interference) $SNR = 13.4716$ dB, $MSE = 0.0153$ (WGN)
Cuomo et al., 2016 [27]	Recursive filtering	Long-term ST	s20011, s20021, s20031, s20041, s20051, s20061, s20071, s20081, s20091, and 20,101	$SNR = 21.28$ dB (s20031)
Mourad, 2019 [28]	Band-pass filter+group sparsity and singular spectrum analysis	Simulated ECG data MIT-BIH	100, 103, 113, 115, 122, 124, and 231	$SNR_{IMP} > 10.00$ dB (5 dB I/P SNR for record) $SNR_{IMP} \geq 10.00$ dB (5 dB I/P SNR for record 103)
Cuomo et al., 2015 [29]	Recursive filter	Long-term ST	s20011, s20051, s20061, s20071, s20081, and s20121	$SNR = 15.88$ dB (s-20061)
Panigrahy and Sahu, 2016 [30]	Phase assignment+template extraction+optimized parameters estimation using differential evolution+extended Kalman smoother	MIT-BIH	100, 103, 104, 105, 106, 115, and 215	$SNR_{IMP} = 1.566742$ dB (avg.), $MSE = 0.017396$ (avg.), $PRD = 46.96928$ (avg.) (at 5 dB I/P SNR for real muscle artifact)
Jenkal et al., 2016 [31]	Discrete wavelet transform+adaptive dual threshold filter	MIT-BIH	100, 101, 103, 113, 115, 117, 119, and 122	$SNR_{IMP} = 9.70$ dB, $PRD = 18.26\%$ , $MSE = 0.0044$ , $RMSE = 0.066$ (for record 100 at 5 dB WGN)

Table 2 (continued)

References	Method	Database	Record	Evaluation parameters
Singh et al., 2017 [32]	Discrete wavelet transform + denoising + reconstruction	MIT-BIH	100, 103, 104, 105, 106, 115, and 215	$SNR_{IMP} \geq 8.00$ dB, $MSE = 0.000893$ , $PRD = 7.75$ (10 dB I/P SNR for record 103)
Lin et al., 2014 [33]	Discrete wavelet transform + soft thresholding	MIT-BIH	All 48 records	$SNR_{IMP} = 11.53$ dB at (0 dB I/P SNR)
Wang and Ji, 2014 [34]	Dual-tree complex wavelet transform	MIT-BIH	100, 101, 102, 103, 104, 105, 106, 107, 108, 109, and 111	$SNR = 55.4198$ dB, $MSE = 0.00063647$ (for record 103)
B'Charri et al., 2017 [35]	Dual-tree complex wavelet transform + hyperbolic thresholding	Synthetic ECG MIT-BIH	100, 101, 102, 103, 104, 105, 106, 107, 108, 109, and 111	$SNR_{IMP} = 10.85304$ dB, $MSE = 0.00120$ (at 5 dB I/P SNR for CN) $SNR = 113.8190$ dB (for record 109)
Zhang et al., 2013 [36]	Wavelet transform + composite threshold	MIT-BIH	124	$SNR = 150.0776$ dB, $MSE = 0.0049$ (for PLI + EMG + BW noise at I/P SNR = 121.7965 dB and $MSE = 0.0222$ )
Peng and Wang, 2017 [37]	Discrete wavelet transform (optimal wavelet)	ECG ID	Person_01/rec_1, Person_02/rec_1, Person_03/rec_1, Person_04/rec_1, Person_05/rec_1, Person_06/rec_1, Person_07/rec_1, Person_08/rec_1, Person_09/rec_1, Person_010/rec_1	$MSE = 0.076$ (avg.), $NSR = 0.0668$
Han and Xu, 2016 [38]	Improved wavelet thresholding (sigmoid function thresholding)	MIT-BIH	100	$SNR_{OUT} = 17.35$ dB, $MSE = 0.00025$ , $PRD = 13.75\%$ (at 10 dB I/P SNR)

Table 2 (continued)

References	Method	Database	Record	Evaluation parameters
Hong and Yonghong, 2018 [39]	Adaptive wavelet thresholding method	Practical ECG signal	150 (Practical ECG signal)	$SNR_e = 3.2225$ , $RMSE_e = 0.0593$ , $r_e = 0.1383$ (avg.)
Kumar et al., 2018 [40]	Wavelet transform	MIT-BIH PTB	16 records (80 + 365) records	$SNR = 30.0051$ dB, $MSE = 0.0008$ (Random Noise) $SNR = 32.6583$ dB, $MSE = 0.0003$ (WGN)
Kumar et al., 2018 [41]	Modified bio-orthogonal 3.1 wavelet transform	BIDMC	15 records	$SNR = 28.3821$ dB, $MSE = 0.0029$ (BWN)
		ST	17 records	$SNR = 30.0051$ dB, $MSE = 0.0008$ (PLI)
		MIT-BIH	48 records	Avg. $SNR = -45.7617$ dB, Avg. $RMSE = 0.008$ , Avg. $PRD = 12.141\%$ (10 s) Avg. $SNR = -45.9406$ dB, Avg. $RMSE = 0.003$ , Avg. $PRD = 11.943\%$ (1 min.) Avg. $SNR = -46.0681$ dB, Avg. $RMSE = 0.002$ , Avg. $PRD = 12.008\%$ (full length) Avg. $SNR = -45.3998$ dB, Avg. $RMSE = 0.008$ , Avg. $PRD = 11.853\%$ (full length) Avg. $SNR = -45.5263$ dB, Avg. $RMSE = 0.002$ , Avg. $PRD = 11.871\%$ (full length) Avg. $SNR = -45.9285$ dB, Avg. $RMSE = 0.003$ , Avg. $PRD = 11.943\%$ (full length) Avg. $SNR = -45.1232$ dB, Avg. $RMSE = 0.006$ , Avg. $PRD = 12.210\%$ (full length)
Smital et al., 2013 [42]	Adaptive wavelet Wiener filtering	Fantasia QT	NA 105 records	Avg. $SNR_{IMP} = 10.6$ dB, $STD_{IMP} = 2.2$ dB
Hao et al., 2017 [43]	Subspace projection + multivariate wavelet denoising	Apnea ECG CSE	NA Whole records	$SNR > 13.5$ dB (for 8 dB I/P SNR)
Kumar et al., 2019 [44]	Three-band biorthogonal wavelet filter bank + adaptive threshold	MIT-BIH	NA	Avg. $SNR > 40$ dB, Avg. $PRD < 5\%$ , Avg. $E_{MA} = 0.0013$ , Avg. $C_R = 22.61$ , Avg. $Q_S = 27.81$ , Avg. $C_T = 327.29$ ms, Avg. $RMSE = 0.0016$
Yadav et al., 2015 [45]	Non-local wavelet transform (similarity data matrix extraction + shrinkage of Transform coefficient and Aggregation)	MIT-BIH PTB	100, 103, 104, 105, 106, 115, and 215 s0032_rem, s0207_rem, s0508_rem, s0510_rem, s0430_rem, s0035_rem, s0354lrem, s0370lrem, s0003_rem, s0012_rem, s0432_rem, and s0390lrem	$SNR_{IMP} > 5$ dB, $PRD > 10\%$ , $MSE \geq 0.002$ (at record 100) $SNR_{IMP} = 18.92$ dB, $PRD = 18.82\%$ , $MSE = 0.0006$ (for record id-s0508_rem)



Table 2 (continued)

References	Method	Database	Record	Evaluation parameters
Tracey and Miller, 2012 [46]	Non-local mean	MIT-BIH	100, 103, 104, 105, 106, 115, and 215	$SNR_{IMP} = 6 \sim 7$ dB, $MSE = 0 \sim 0.01$ , $PRD < 20\%$ (at 15 dB I/P SNR)
Qian et al., 2019 [47]	Noise estimation and local mean denoising	MIT-BIH Long term ST	100, 103, 104, 105, 106, 115, and 215 s20011, s20021, s20031, s20041, s20051, s20061, s20071, s20081, s20091, and s20101	$SNR_{IMP} > 10$ dB, $MSE < 0.004$ , $PRD > 12\%$ (at 6 dB I/P SNR) $SNR_{IMP} > 8$ dB, $MSE < 0.005$ , $PRD > 12\%$ (at 6 dB I/P SNR)
Anapagmini and Rajavel, 2016 [48]	Empirical mode decomposition + power line interference removal + detector	MIT-BIH	106	$RMSE = 11.9$ , $CC = 0.9884$  $RMSE = 6.87$ , $CC = 0.9883$
			121	$RMSE = 5.58$ , $CC = 0.9902$  $RMSE = 12.01$ , $CC = 0.9872$ (DSP implementation) $RMSE = 06.92$ , $CC = 0.9840$ (DSP implementation) $RMSE = 5.83$ , $CC = 0.9900$ (DSP implementation)
Jain et al., 2018 [49]	Empirical mode decomposition + Savitzky-Golay filtering + Riemann Liouville fractional integral + median filtering	MIT-BIH	115	$SNR_{IMP} = 7.5288$ dB, $MSE = 0.0027$ (AWGN) $SNR_{IMP} = 10.6116$ dB, $MSE = 0.0013$ (MA) $SNR_{IMP} = 12.0526$ dB, $MSE = 0.00096$ (PLI) $SNR_{IMP} = 7.6487$ dB, $MSE = 0.0026$ (BWN)
Kumar et al., 2018 [50]	Empirical mode decomposition + non-local mean	MIT-BIH	100, 103, 105, 106, 115, and 215	$SNR_{IMP} \geq 10$ dB, $PRD > 50\%$ , $MSE < 0.01$ (for record 100 at -5 dB SNR with AWGN)

Table 2 (continued)

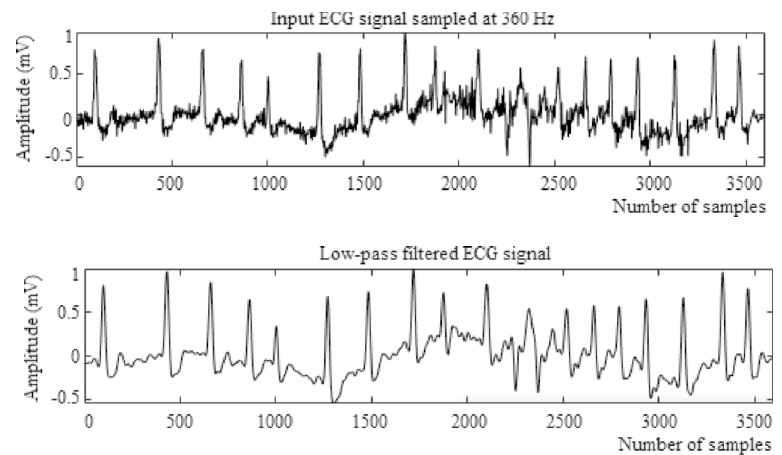
References	Method	Database	Record	Evaluation parameters
Rakshit and Das, 2018 [51]	Empirical mode decomposition + adaptive switching mean filter	MIT-BIH	100, 101, 103, 105, 115, 200, 215, and 230	$SNR_{IMP} = 9.2980$ dB, PRD = 34.3190%, MSE = 0.02022. (at 0 dB I/P SNR)
Kabir and Shahmaz, 2012 [52]	Empirical mode decomposition + windowing + wavelet with soft thresholding	MIT-BIH	07	$SNR_{IMP} > 6$ dB (at 15 dB I/P SNR), PRD > 10, MSE = 0.0019 (at record 100)
Singh et al., 2018 [53]	Non-local mean + modified empirical mode decomposition	MIT-BIH	100, 103, 104, 105, 106, 115, and 215	$SNR_{IMP} \approx 8$ dB, PRD > 8%, MSE = 0.000464 (at 10 dB I/P SNR for record 100)
Jain et al., 2018 [54]	Ensemble empirical mode decomposition + particle swarm optimization algorithm (PSO) + cuckoo search (CS) optimization algorithm	MIT-BIH	115	$SNR_{IMP} = 10.0809$ dB, MSE = 0.0015 (Random Noise)
Wang et al., 2019 [55]	Improved complete ensemble empirical mode decomposition-zero-crossing scale thresholding	MIT-BIH	100	$SNR_{OUT} = 22.2600$ dB, RMSE = 0.0315 (at 15 dB I/P SNR)
Das and Ari, 2013 [56]	S transform and thresholding	MIT-BIH	100, 101, 102, 103, 113, 201, 207, 214, 217, and 231	$SNR = 9.44$ dB, RMSE = 0.1024 and PRD $\approx 30\%$ (for record number 113 at 5 dB input SNR)
Singhal et al., 2020 [57]	Fourier decomposition method	MIT-BIH	100, 101, 103, 105, 109, 111, 112, 113, 115, 116, 117, 118, 122, 123, 210, and 212	$SNR_{OUT} = 28.5$ dB, PRD > 0 (for 5 dB I/P SNR and record 100) (60 Hz PLI) $SNR_{OUT} = 23.0$ dB, PRD > 5% (for 5 dB I/P SNR and record 100) (BW) $SNR_{OUT} = 23.3$ dB, PRD > 5 (for 5 dB I/P SNR and record 100) (60 Hz PLI + BW)

Table 2 (continued)

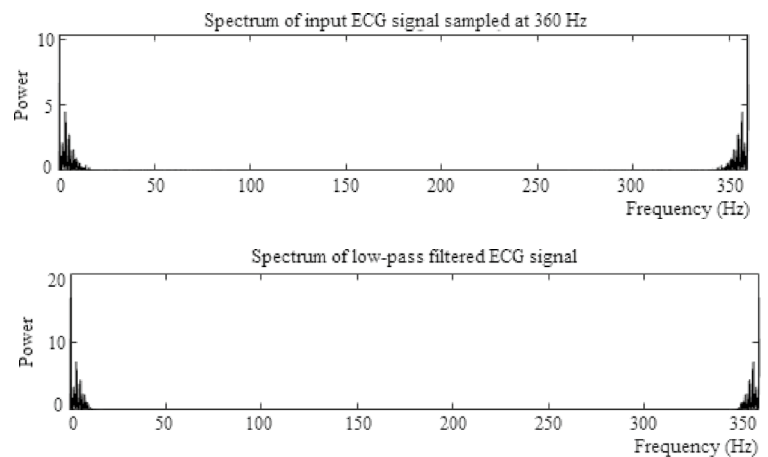
References	Method	Database	Record	Evaluation parameters
Tan et al., 2019 [58]	Blaschke unwinding adaptive Fourier decomposition	MIT-BIH	All 48 records	SNR = 31.05 dB, PRD = 1.47%, CR = 35.53, QS = 32.58
Sharma and Pachori, 2018 [59]	Eigenvalue decomposition of Hankel matrix	MIT-BIH	100, 101, 103, 105, 108, 109, 111, 112, 113, 115, 116, 117, 118, 121, 122, 123, 210, and 212	SNR <sub>OUT</sub> = 11.52 dB, PRD ≥ 20% (for record 100)
Kumar et al., 2021 [60]	Stationary wavelet transform	MIT-BIH	100, 101, 102, 103, 104, 105, 109, 112, 117, 118, 123, 200, 205, 213, 221, 231, and 234	SNR <sub>OUT</sub> = 49.35 dB, RMSE = 0.0006, PRD = 0.254 (for record 100 at 14.32 dB I/P SNR)
Prashar et al., 2021 [61]	High-pass filter + dual tree complex wavelet transform	MIT-BIH	All 48 records	SNR = 58.23 dB, MSE = 0.0000000963, PRD = 0.001 (for record 100)

\* QS Compression efficiency, CC correlation coefficient, STD standard deviation, NSR noise suppression ratio

**Fig. 5** Effect of LPF on ECG Signal (a) Input ECG signal and its low-pass filtered version (b) Spectrum of input ECG signal and low-pass filtered ECG signal



(a) Input ECG signal and its low-pass filtered version



(b) Spectrum of input ECG signal and low-pass filtered ECG signal

while the spectrum of the original ECG record and low-pass filtered signal is shown in Fig. 5b. The power is normalized in the Figures. The cut-off frequency of LPF is about 11 Hz. Although the LPF removes the high-frequency noises like PLI and many more, it also attenuates the ECG amplitude and distorts some significant ECG characteristics.

The low-pass filter significantly affects the ECG signal, so various researchers proposed a high-pass filter as an alternative for noise elimination. HPF being simple, easily implementable, is used to remove baseline wander, DC offset, and drift suppression [66]. HPF with cut-off frequencies of 0.05 Hz, 0.5 Hz, 1 Hz, and 2.2 Hz is used frequently to remove baseline wander and drift. The effect of HPF on the MIT-BIH record 203, in both the time-domain and frequency-domain, is demonstrated in Fig. 6. The cut-off frequency for this high-pass filtering operation is 5 Hz. Figure 6 shows that the HPF removes the DC offset and minimizes the baseline wander noise. Since all the heart information lies in a frequency range, researchers are interested in using a band-pass filter for pre-processing. BPF is used

to eliminate different kinds of noise like baseline wander, EMG, PLI, and other low and high-frequency noise components. Various authors use different frequency range for BPF which are: 0.5–40 Hz, 1–30 Hz, 0.05–40 Hz, 1–100 Hz [67–70]. The response of a typical BPF with cut-off frequency 5–15 Hz for MIT-BIH record 203 is shown in Fig. 7. The time-domain and frequency-domain responses in Fig. 7 show that the BPF enhances the QRS complex characteristics by eliminating low and high-frequency noises.

Along with many advantageous features, the band-pass filter suffers from some disadvantages also. There are two important features of a band-pass filter. First, the BPF output may contain some artifacts and ripple due to low-frequency components. Second, it is challenging to select cut-off frequencies that do not overlap with the desired ECG signal [71]. In [28], Mourad combined group sparsity and singular spectrum algorithm (GSSSA) with BPF for ECG signal denoising. The block diagram of a typical filtering method, based on low-pass and high-pass filtering for ECG signal analysis, is shown in Fig. 8.

**Fig. 6** Effect of HPF on ECG signal

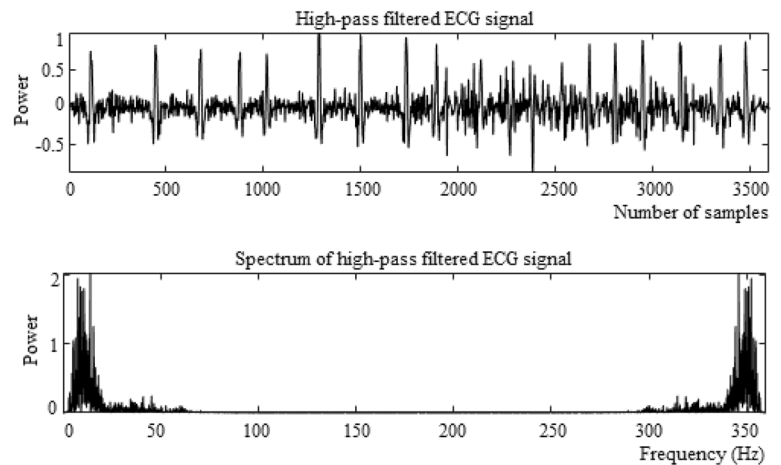


**Fig. 7** Effect of BPF on ECG signal

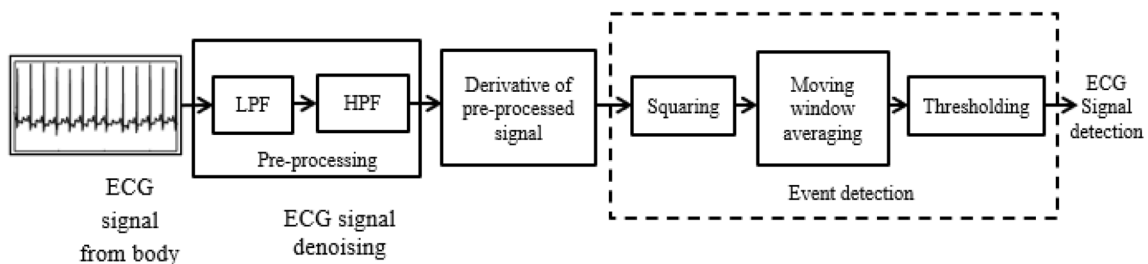
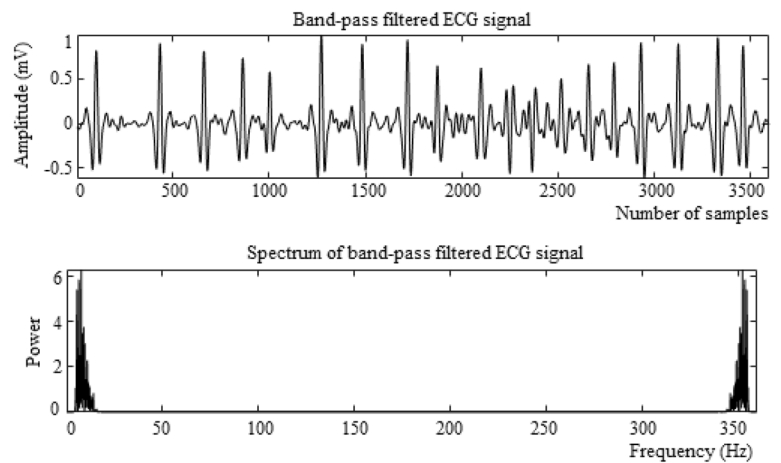


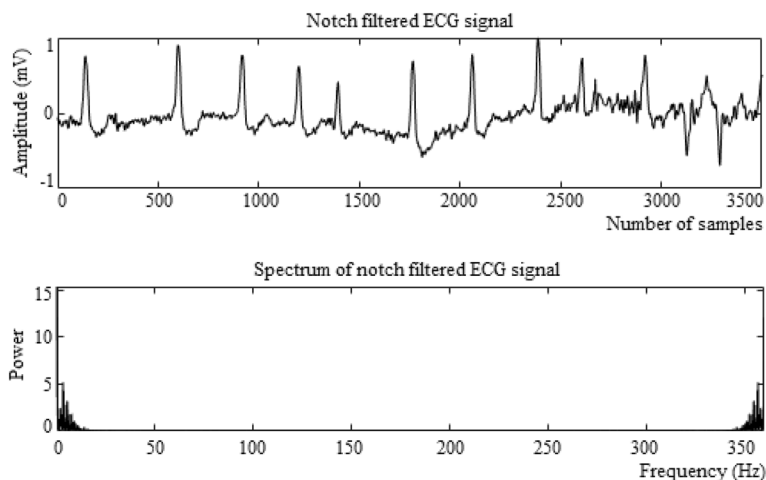
**Fig. 8** The filtering method of ECG signal analysis

Above mentioned filters can remove a range of frequencies, but sometimes removing a single frequency is necessary. A notch filter is popularly used to remove a single frequency component like PLI (50 or 60 Hz) [7, 72]. A notch filter is a band-stop filter of a very narrow bandwidth. A good quality notch filter should attenuate the targeted frequency and preserve the rest. Various research groups use a notch filter with 50 or 60 Hz center frequency to remove the power line interference. Although a notch filter preserves

the other frequencies for rapidly changing waveform, they produce unusual ringing.

Notch filters are suitable for removing a single frequency noise, but other noises cannot be removed simultaneously [73]. The effect of the notch filter on MIT-BIH arrhythmia record 203 is shown in Fig. 9. As the ECG signal contains some impulsive noises, their presence may lead to false detection of QRS complex or R-peak. Conventional filters like LPF and HPF cannot remove impulsive noises. Hence

**Fig. 9** Effect of notch filter on ECG signal



many researchers propose a median filter as an attractive tool to remove impulsive noise while preserving signal edges. A median filter is a non-linear digital filter used to remove noises from the images and signals.

Median filtering has unique advantages over linear filtering techniques. The linear filter cannot handle impulsive noise (sharp discontinuities of small duration) without altering the signal characteristics [74]. The median filter operates on the signal, entry by entry, and replaces every entry by the median of neighboring entries. The neighboring pattern is called a window, which slides over the entire signal. Generally, median filters with a window size of 200 to 600 ms are used to restore the baseline of an ECG signal. In the median filter, the predicted value of the current point depends on the past and future values. A median filter removes the baseline wander by assuming that the ECG signal and baseline wander have different amplitude distributions within the window. A median filter's main drawback is a longer computational time for wide window width and complex behavior.

During filtering, preserving the shape of the ECG waveform is essential as the shape contains crucial information on cardiac health. Savitsky–Golay's (S–G) filtering scheme removes noise and preserves the waveform shape. This filtering scheme based on the least square polynomial approximation method draws the attention of many researchers. Preserving the peak height and width of the signal waveform in a noisy environment makes S–G filtering an attractive choice for ECG signal analysis. S–G filters are low-pass filters obtained by fitting a polynomial to the input samples sequence and calculating that polynomial at a point within the selected interval. An extremely flat passband and moderate attenuation in the stopband of an S–G filter help achieve excellent results. In S–G filtering, the computational time is proportional to window width, so window width must be appropriately selected. S–G filters are useful in those applications where signal spectrum and noise overlap with each other. This fact of the S–G filter is used to remove the

baseline drift in the ECG signal. The denoising accuracy of an S–G filter depends on the frame length and order of the polynomials. In an S–G filter, the frame length and order of the polynomial are determined by experimentation, which is a disadvantage of the S–G filter [75].

All the filters mentioned above require some prior knowledge about signal or noise. Based on this knowledge, the filters are designed for a particular task and thus categorized as fixed filters. A fixed filter requires a new design whenever there is a change in the input or any other condition. An adaptive filter resolves the problem of a fixed filter. Adaptive filters can automatically adjust the filter coefficients according to the specific requirement. Unlike a fixed filter, the design of an adaptive filter requires little or no prior knowledge of input or noise [76]. The adaptive filter minimizes the mean squared error between the primary input and a reference signal. Generally, the primary input is a noisy ECG signal, and the reference signal is either noise or a signal correlated with noise or ECG signal in primary input, respectively. Easy implementation of advanced hardware or microcontrollers with digital numerical capabilities makes adaptive filters suitable for the digital environment [77]. Based on requirements, various algorithms like least mean square (LMS), normalized least mean square (NLMS), recursive least square (RLS), sign-LMS, and sign-sign LMS are used to design adaptive filters. LMS algorithm has the advantages of implementation simplicity and tracking the statistical changes of non-stationary signals. In contrast, the RMS algorithm offers a faster convergence rate at the cost of increased computational complexity.

Based on the computational unit used to implement an adaptive filter, the filters are categorized as linear and non-linear adaptive filters. In a linear adaptive filter, the output is a linear combination of the observations applied to the input of the filter. The linear adaptive filter has a single computational unit for each output. Linear adaptive filtering is not capable of exploring the higher-order statistics of input data.

On the other hand, non-linear adaptive filtering uses non-linear computational units to explore the complete information contained in the input signal. Non-linear components in non-linear adaptive filtering make mathematical analysis much more complicated than linear filtering methods. Adaptive filtering is useful in removing motion artifacts, PLI, baseline wander, and EMG [77]. Although adaptive filtering has numerous advantages, the main drawback is the reference signal requirement, as the choice of the reference signal may significantly affect the efficiency of the method [78, 79].

Many researchers used a moving average filter in ECG signal processing due to its simplicity and ease of use. Moving average filter is a finite impulse response filter used to minimize the random noise while maintaining a sharp step response. The idea behind the moving average filter is to take samples from the input dataset at predefined intervals and take the average of that input to produce an output. This process is repeated over the entire dataset, and a line, known as moving average, is constructed by connecting all these averages. The moving average filter loses the inter-beat information due to averaging. The moving average filter is more suitable for time-domain encoded signals. Moving average filter is unsuitable for a frequency-domain encoded signal as it cannot separate one frequency band from the other [80]. While denoising, the edge-preservation of the ECG signal is essential, so some researchers found non-local mean filtering (NLM) suitable for denoising the ECG signal. Non-local mean (NLM) filtering was initially used for 2D image processing later; various researchers use it to denoise biomedical signals like ECG and EEG [24, 81]. Tracey and Miller first used the non-local mean denoising technique [46] for ECG signal denoising.

The non-local mean filtering is a patch-based method that calculates the weighted sum of a patch. NLM filter uses neighboring and non-neighboring patches for weight calculation. Based on this weighted sum, the noise is filtered out. Although the NLM filtering provides good denoising results and preserves the edges of an ECG signal, computational complexity increases the computational cost [46]. Lee and Hwang [24] adapted pNLM filtering with HPF and LPF to denoise selected ECG records from the MIT-BIH database and achieved an average SNR improvement of 7.67 dB.

The filtering techniques mentioned above are off-line methods where the ECG signals are recorded first and then denoised to improve the quality of the signal. However, in real-time applications, where the ECG data are provided by wearable sensors and transmitted to mobile devices, these methods show inefficacy. A real-time ECG signal processing requires computationally efficient filtering schemes. A recursive filter (RF) provides computational efficiency in computing time and memory usage [27]. A recursive filter is an infinite impulse response (IIR) filter whose output is a linear combination of present input and previous inputs

and outputs. Recursive filtering provides low computational cost, fast operation, steeper selectivity, large gain with fewer sections. The main drawback of this method is its practical implementation due to the nonconvex optimization problem [82]. Cuomo et al. [27, 29] used recursive filtering for denoising the ECG signal.

Another edge-preserving denoising method is the Kalman filter (KF). It is a powerful tool to estimate the hidden state of a system with the help of a dynamic model of the system and measured data. KF deals effectively with noisy data and with random external factors. It assumes a linear relationship between the system dynamics and measured data. As most of the systems are non-linear, variants of KF are used to analyze non-linear systems. The popular variants of extended Kalman filter (EKF) are unscented Kalman filter (UKF) and extended Kalman smoother (EKS). EKF is an extension of KF for a non-linear system that assumes a non-linear relationship between measured data and the system. The purpose of EKF is the linearization of the non-linear system model close to the previously estimated points. EKF is not an optimal filter like KF. UKF method uses an unscented transform (UT) to denoise an ECG signal. The estimated covariance and sensitive matrices using UT are semidefinite. Hence it is difficult to realize a numerically stable UKF system to cancel noise in an ECG signal.

The EKS denoising method is a non-causal approach as it utilizes future observations to estimate the present state. EKS consists of two stages: the forward EKF stage and the backward recursive smoothing stage. The non-causal nature of EKS provides better performance as compared to EKF [83]. Denoising techniques based on EKF, UKF, and EKS provide better denoising results. However, sometimes these methods require operator interaction to initialize parameters such as amplitude, phase, and width to estimate an ECG signal [30]. EKS, along with differential evolution (DE), is proposed by Panigrahy and Sahu [30] for denoising, but this approach may provide a lower performance at a low sampling rate of ECG signal. As mentioned above, the researchers used various filtering techniques and achieved ECG detection accuracy greater than 99%.

Generally, Butterworth filters are preferred for medical applications due to their maximally flat magnitude response, less computational cost, and accuracy. IIR Butterworth filter has a better frequency than finite impulse (FIR) filter [84]. The filtering techniques suffer from many drawbacks, such as the ringing effect and lack of information on the signal's frequency content. The filtering technique also affects the waveform of the ECG signal. Frequency-domain techniques remove some of these drawbacks. Popular frequency-domain techniques are discrete Fourier transform (DFT), fast Fourier transform (FFT), discrete cosine transform (DCT). These techniques provide the frequency content of the signal. The earliest technique is DFT, which converts the time-domain

samples into the frequency domain. DFT is not a function of any variable, but it is a sequence. DFT decomposes the signal in terms of orthogonal sine and cosine functions of different frequencies. These individual components of the signal can be easily analyzed and processed compared to the original signal [85]. For  $N$  samples, namely  $x(0), x(1), x(2) \dots x(k) \dots x(N-1)$  of a signal  $x(n)$ , the  $N$ -point DFT of the signal is given by (1).

$$X(k) = \sum_{n=0}^{N-1} x(n)W_N^{kn}, \quad 0 \leq k \leq N-1 \quad (1)$$

Here  $W_N = e^{-\frac{j2\pi}{N}}$  is known as the twiddle factor.

DFT is a powerful tool for providing spectral information of the signal. DFT deals with finite data points; it is easy to implement DFT in computers with numerical algorithms. DFT involves many calculations, so a fast-computational algorithm, called fast Fourier transform (FFT), is developed. FFT is a tool to perform DFT efficiently [86]. DFT requires  $N^2$  multiplications and  $N(N-1)$  additions for a data sequence of  $N$ -points, whereas FFT requires  $\frac{N}{2}(\log_2 N)$  multiplications and  $N \log_2(N)$  additions [29, 87, 88]. By using the FFT algorithm, Kumar et al. [88] achieved a sensitivity of 99.65%. Noor et al. [89] achieved low energy consumption by using FFT.

Figure 10 shows a frequency-domain based method to analyze ECG signals, where an analysis filter bank is used to pre-process the signal. When operated on non-stationary signals, DFT/FFT fails to provide information about instantaneous frequency. Further, one cannot apply DFT/FFT to a multichannel signal. Other frequency-domain techniques like discrete cosine transform (DCT) can express a discrete-time-domain signal into a sum of cosine functions having different frequencies. Due to the energy compaction property, DCT is used for ECG compression [90–92]. The major disadvantage of DCT is the requirement of the quantization step to get an integer-valued output [93].

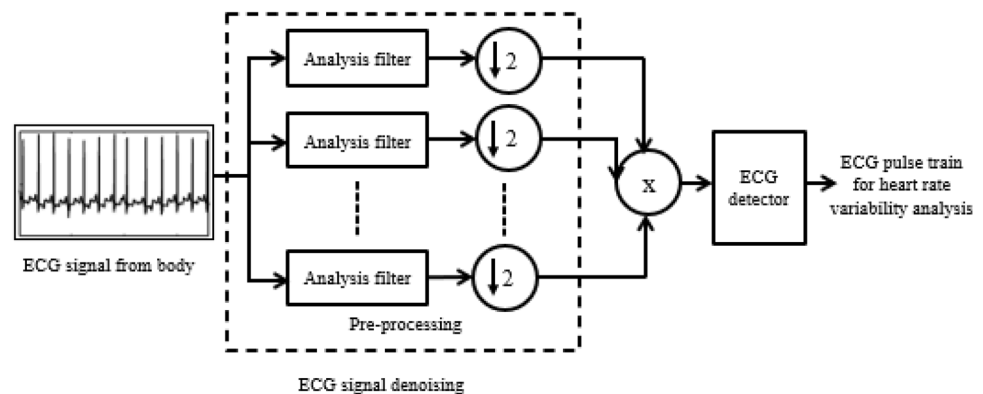
Although these frequency-domain techniques provide spectral information of an ECG signal, they do not provide

temporal information. ECG signal, being non-stationary, possesses highly complex time–frequency characteristics, and they cannot be analyzed only using time or frequency-domain techniques. Short-time Fourier transform (STFT), introduced by Gabor in 1946, is a technique that combines both the time and frequency component analysis, which enables a comprehensive analysis of an ECG signal [94]. STFT provides time localized frequency information for a situation in which the frequency component of a signal varies with time [94, 95]. In STFT, with the help of a moving, fixed-width time window, multiple frames of the signal are extracted, and after then, Fourier transform is applied to get the frequency information of these multiple frames. The size of the window is narrow so that the frame would appear stationary. Thus, STFT eliminates the limitation of the Fourier transform by providing both time and frequency information. Xie et al. [96] achieved a classification accuracy of 98.4% using STFT. The main limitation of STFT is a trade-off between time and frequency resolution. Selecting a narrow time window provides a good time resolution but degrades the frequency resolution.

Similarly, a broader time window degrades the time resolution but improves the frequency resolution. Further, a fixed window length imposes a limit on non-stationary information extracted from the signal. A wavelet transform reduces the limitations imposed by STFT. Wavelet transform improves the time–frequency resolution by varying the window length. The flexible window length of wavelet transform helps obtain long, low-frequency, and small, high-frequency information simultaneously. In wavelet transform, a set of basis functions known as a wavelet represent the signal. A wavelet is a waveform with a limited duration and zero average value. A function with the following criteria can be used as a wavelet [97].

- (i) It must have finite energy.
- (ii) A function with a no zero-frequency component, or it must have zero mean.

**Fig. 10** ECG signal analysis using filter bank method





- (iii) Fourier transform of a complex function must be real and zero for negative frequencies.

Various researchers used different wavelets like Daubechies wavelets, Symlet wavelets, Haar wavelet, Biorthogonal wavelet, Coiflet wavelets, Meyer wavelet to decompose an ECG signal. The type of wavelet to be used is determined by the application [40]. Wavelet transform can be classified into discrete wavelet transform (DWT) and continuous wavelet transform (CWT). DWT decomposes the signal into a set of functions that are orthogonal to its translation and scaling coefficient. On the other hand, CWT provides an output vector larger by one dimension than the input signal. CWT uses non-orthogonal wavelets, which provide highly correlated output vector values. The use of non-orthogonal wavelets in CWT improves the visualization of signals in higher dimensions, but it is not very useful for classification. Sabherwal et al. [98], Sahoo et al. [99], and Banerjee et al. [100] used Daubechies-6 (dB6), Rakshit and Das [101] used *dB10* wavelet, Park et al. [102] used Symlets wavelet (sym5). Li et al. [103] used a quadratic spline wavelet as a mother wavelet for ECG signal denoising. Sabherwal et al. [98], Sahoo et al. [99], Banerjee et al. [100], and Li et al. [104] achieved a sensitivity greater than 99.5% using wavelet transform. Rakshit and Das [101], Park et al. [102], Yochum et al. [105], and Sabherwal et al. [106] have gained a sensitivity of 99.93%, 99.93%, 99.87%, and 99.99%, respectively.

The principle of the wavelet transform for ECG signal analysis is represented in Fig. 11. The wavelet decomposer decomposes the ECG signal into wavelet coefficients. With the help of these wavelet coefficients, the denoised ECG signal is generated for further analysis of heart rate variability.

The effect of the wavelet transform on a typical MIT-BIH record 109 is shown in Fig. 12. Figure 12 demonstrates that the wavelet transform has successfully removed the baseline wander noise, EMG, and others. Although wavelet transform has many advantages over other techniques like filtering, Fourier transforms, there are still some drawbacks. First, it is not able to capture the edges adequately. Second, a trade-off exists between accuracy and computational time. A significant drawback of wavelet transform is low directional selectivity. The selection of the basis function in the wavelet transform is also a rigorous task. Some drawbacks of wavelet transform are removed by empirical mode decomposition (EMD) by decomposing the signal into intrinsic mode functions (IMF) [49–51, 107]. The basic concept of EMD is to identify proper time scales that reveals the physical characteristic of the signal and then decompose the signal into modes intrinsic to the function, referred to as IMF. IMFs are signals that satisfy the following criteria:

- (i) In the whole data set, the difference between the number of extrema and zero-crossing count must be either equal to zero or differ by one.
- (ii) At any point, the mean value of the envelope defined by local maxima and envelope defined by local minima is zero.

The number of IMF depends on the length of the ECG segment. A long ECG segment produces a large number of IMF. EMD is an iterative process. The iterations can be converged by imposing conditions like standard deviation, the amplitude of the remaining signal, mean value of the

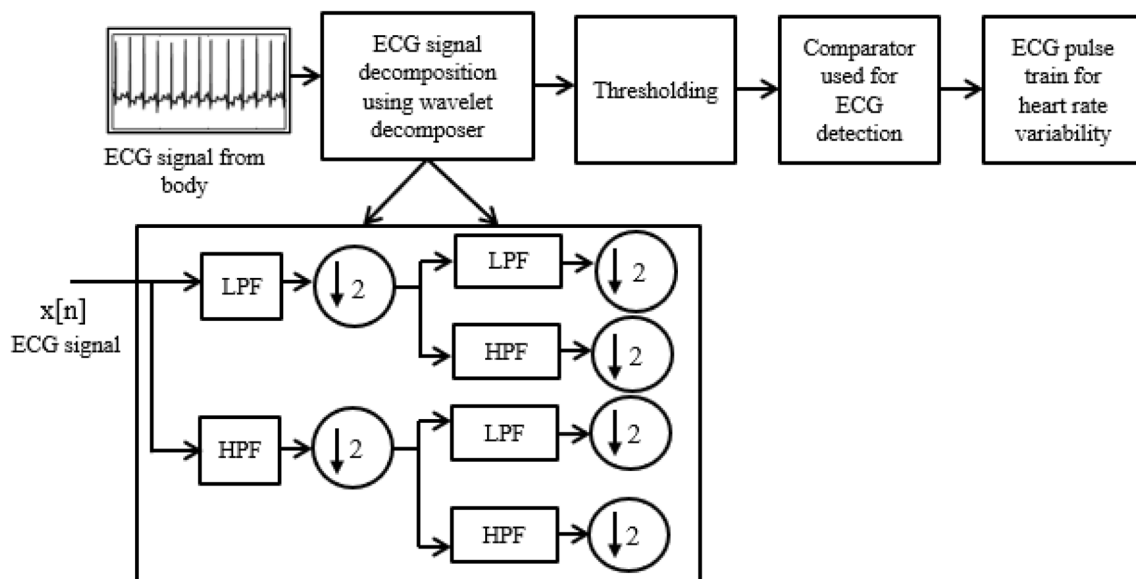
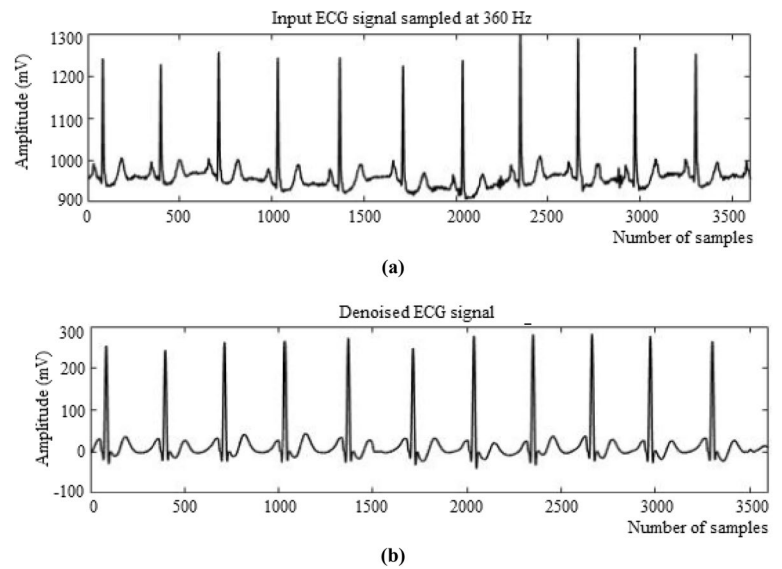


Fig. 11 ECG signal analysis using the wavelet transform

**Fig. 12** a Input ECG signal b denoised ECG signal



envelope, cross-correlation coefficient between the original signal and the remaining signal. EMD is a model-free, entirely data-driven method that naturally copes with non-stationarities and non-linearities. EMD based algorithms are helpful for the removal of baseline wander and high-frequency noise. A typical EMD algorithm is a multi-step process and is simple to implement. EMD uses several equations to extract various features of an ECG signal. EMD is one of the most relevant techniques to remove respiratory signals from the single-channel ECG recording [108, 109]. Rakshit and Das [51], Kabir and Shahnaz [52] utilized EMD for denoising the ECG signal and achieved an SNR improvement of 9.29 dB and greater than 6 dB, respectively. The drawbacks of the EMD technique are a deficiency of theoretical background and mode mixing.

The block diagram of the EMD based ECG signal denoising system is shown in Fig. 13. The EMD method decomposes the ECG signal into many IMFs. The IMF corresponding to various noises is discarded to obtain the clean ECG signal. Denoised ECG signal is then used to detect various events like P-wave, QRS complex, R peak, T wave. A typical ECG record taken from MIT-BIH and its IMFs obtained from EMD operation are presented in Fig. 14. The ECG signal is decomposed into eight IMFs and a residue signal. From IMF1 to the residue signal, the oscillatory behavior is decreasing continuously. The lower order IMFs represent the high-frequency components of the signal, and noise is spread over these IMFs. EMD suffers from a significant drawback, known as mode mixing. In mode mixing, oscillations from different time scales appear in a given IMF, or oscillations from the same scale appear in different IMFs [110]. Like the wavelet transform, EMD is also not able to preserve the edges. Also, the lack of a theoretical framework is another major problem of EMD. Wu and Huang [111] introduced a

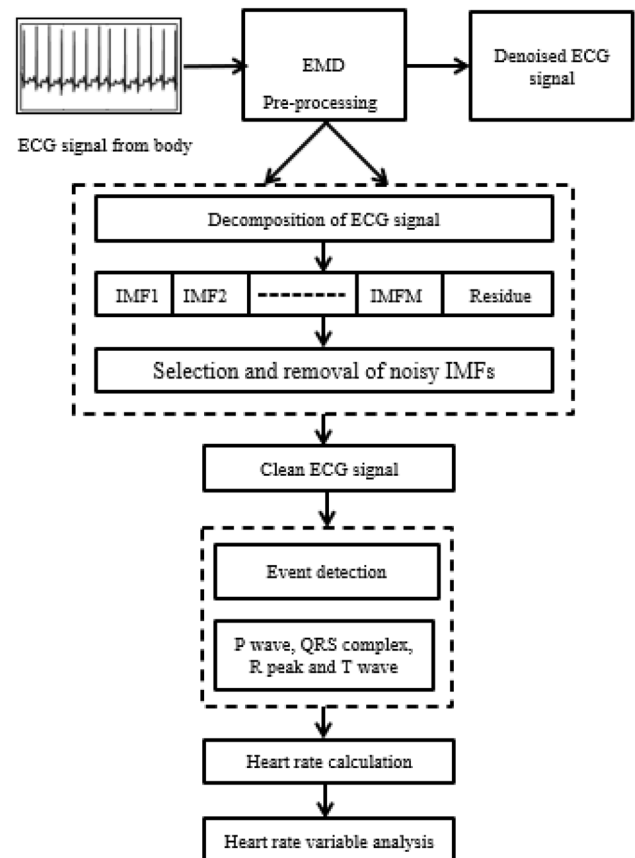
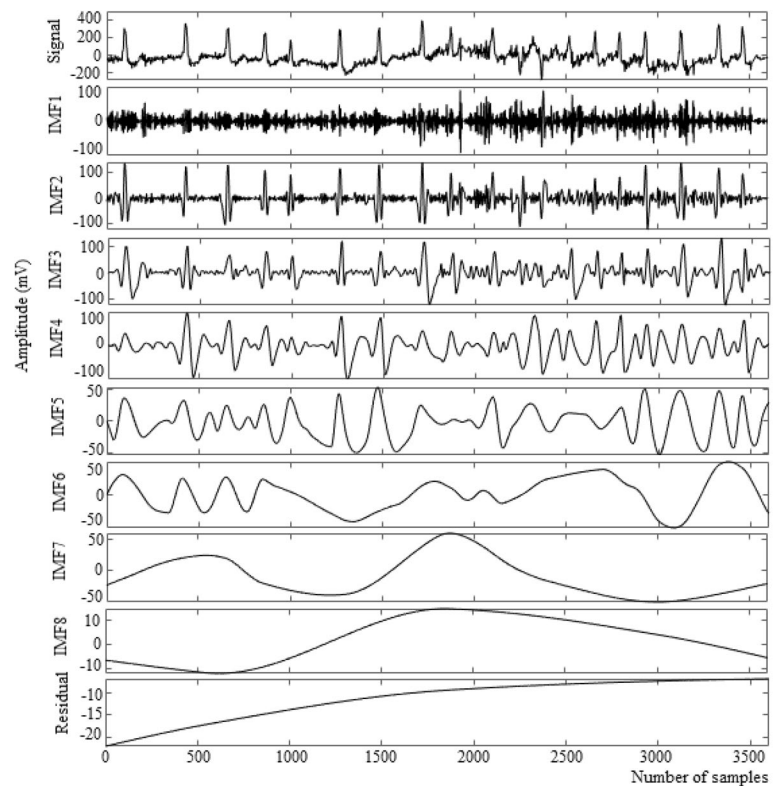


**Fig. 13** ECG signal analysis with the help of the EMD method

new technique known as ensemble empirical mode decomposition (EEMD) to eliminate the mode mixing problem of EMD. EEMD is a noise-assisted EMD algorithm. In EEMD, different series of white noise are added to the original signal

**Fig. 14** Input ECG signal and the eight IMFs after EMD decomposition



in many trials. Since the noise is different in each trial, the resulting IMFs differ from each trial, which does not exhibit any correlation. If the number of trials is adequate, the added noise can be eliminated from the ensembles by averaging the IMFs from different trials [112, 113]. The number of ensembles and the noise amplitude are required to define an EEMD. Jain et al. [54] achieved an SNR improvement of 10.08 dB for MIT-BIH record number 115. Chang [110], Rajesh and Dhuli [114], Jebaraj and Arumugam [115] demonstrated EEMD as a powerful tool to denoise an ECG signal. Although EEMD provides a significant improvement over EMD, it still suffers from some problems [111]. (i) In EEMD, each trail produces a set of IMFs. The addition of these IMFs does not need to be a true IMF. (ii) IMFs do not provide any information on handling the multi-mode distribution (iii) higher computational complexity.

Variational mode decomposition (VMD) is an enhanced version of EMD used to analyze the non-stationary and non-linear signals. Like EMD, VMD also decomposes the signal into a set of bandlimited amplitude and frequency modulated oscillations known as modes. All the modes have specific sparsity properties to reproduce the signal. The bandwidth of all the modes in the spectral domain is regarded as sparsity. The high operational efficiency of VMD is based on its robust mathematical theory. VMD avoids information loss because it reconstructs a good signal from decomposed

signals. Maji et al. [116] used VMD for QRS detection and achieved a sensitivity of 99.46% with the MIT-BIH database. VMD has some superiority over EMD because the EMD algorithm includes extrema finding, interpolation, and stopping criterion. Any false maxima detection may generate a wrong decomposition, but in VMD, the signal is decomposed around the center frequency of modes. EMD may decompose the ECG signal into unnecessary modes because the decomposition level is independent of the user, but VMD has a controlled decomposition.

The most advantageous feature of VMD is the center frequency of the mode that helps in the characterization of the modes. VMD also provides features like phase angle, which helps categorize the heart rhythm with abnormalities [116, 117]. Various researchers use statistical techniques like principal component analysis (PCA) and independent component analysis (ICA) to denoise the ECG signal. PCA and ICA remove the in-band noise of the ECG signal by removing the dimensions which correspond to noise [118]. They (PCA, ICA) do not show good results with single-lead ECG recordings because these techniques are based on correlation and uncorrelation concepts [119]. Although the techniques mentioned above provide excellent results, the reliability of these techniques for real-time applications requires extensive validation.

## 4 Detection Techniques

In ECG, a complete heart cycle comprises three main events: P-wave, QRS complex, and T wave. Each event has its characteristic peak amplitude, duration, and frequency. It is necessary to detect the events mentioned above properly and accurately to diagnose CVDs and arrhythmias. After detecting any event, the corresponding signal can be analyzed for the peak amplitude, QRS complex width, frequency content, energy, and the interval between events. Accurate detection of a P-wave, QRS complex, and T wave enables accurate analysis of the ECG signal. Over several years, various researchers have focused their investigations on the QRS complex detection as detecting the P-wave and the T wave is quite difficult compared to QRS complex detection. The accurate detection of the P-wave and the T wave is difficult because of their low amplitude, morphology and amplitude variability, low SNR, and sometimes an overlapping between the P-wave and the T wave. Also, from the clinical point of view, detecting the QRS complex is crucial because the multiple premature QRS complexes indicate cardiac dysfunction. Various researchers proposed different methods to detect QRS complex detection [88, 120–132]. However, to date, none of the algorithms can detect all possible variations in a QRS complex due to its complex morphology and noisy ECG signal.

QRS complex detection is a two-step process that includes the pre-processing and decision stage. The pre-processing stage, as mentioned above in Sect. 3, is used for noise removal. After noise removal, the denoised signal is subjected to the decision stage. As shown in Table 3, many detection techniques are proposed in the literature to detect QRS complex and R-peak. These techniques include thresholding, zero-crossing detection (ZCD), syntactic methods, matched filter, mathematical morphology, hidden Markov process, and singularity techniques. Also, to reduce false-positive detection, almost all algorithms use the addition decision rule. Two essential criteria, complexity and performance, are used in the selection of a detection technique. Relatively simple algorithms are used in practice. The performance criterion was used to reject those detection techniques, which gave a large number of false-positive at low noises levels [14].

The simple and widely used detection method is a thresholding technique in which a feature of the pre-processed signal is compared with a fixed or adaptive threshold to detect the QRS complex. The thresholding technique can be applied in time as well as the time–frequency domain. Fixed thresholding is simple and provides a good result for stationary ECG signals, where beat-to-beat morphology does not change.

However, due to noise and baseline wander, ECG signal beat-to-beat morphology changes, and the probability of accurate detection of QRS complex decreases with fixed thresholding. The adaptive threshold [94, 123, 134–136, 145] increases the probability of accurate detection of QRS complexes.

Various researchers [13, 133–136] have used filtering before thresholding to attenuate various noises like PLI, baseline wander, MA, and other signal components like P-wave and T wave. Usually, a band-pass filter is used in the pre-processing stage, but other filters like low-pass [94, 144], high-pass, median, and moving average [122, 146] are used. In [123], a high-pass filter called the MaMeMi filter removes noise from the ECG signal. Using the MaMeMi filter and adaptive threshold, Rufas and Carrabina [123] have obtained a sensitivity of 99.43%. Christov [122] employed a moving average filter and combined threshold (adaptive steep-slope threshold + adaptive integrating threshold + adaptive beat expectation thresholds) for QRS complex detection. Bajaj and Kumar [162] proposed a QRS detection algorithm that uses the concept of Stockwell transform (ST) and fractional Fourier transform along with thresholding. Although the thresholding technique is simple but setting multiple empirical thresholds is the main drawback of this technique. When a beat does not appear for a long time in a threshold-based detection method, the search back mechanism is activated, producing many false beats.

In the wavelet-based detection method used by various researchers [103, 105, 154], the raw ECG signal is decomposed into many coefficients. Only those coefficients that coincide with the QRS complex are selected. The wavelet-based detection method has two limitations: (a) unavailability of a universal rule for selecting mother wavelet (b) effectiveness of the method depends on the level of decomposition. A wavelet-based algorithm can be realized by using an integrated circuit with a detection accuracy of 99%. In [167], Coast et al. proposed a hidden Markov model for QRS complex detection. In hidden Markov modeling, the observed data sequence is characterized by a probability density function that varies with the state of the underlying Markov chain. The Markov chain in hidden Markov modeling models the observed sequence, waveform duration, and intervals within each beat. The Markov chain preserves the structural properties of the underlying process, and state parameters represent the probabilistic nature of the observed data. Hidden Markov modeling offers excellent flexibility in the selection of observation sequences. The problems associated with hidden Markov modeling are computational complexity; many parameters need to be set and manual segmentation for training before analyzing a record [168].

Artificial neural networks (ANN) are useful for the detection and classification of the QRS complexes. As the name suggests, ANN is a computational algorithm based on the

**Table 3** Overview of studies conducted on ECG signal detection

Authors	Technique used to design the algorithm	Feature detected	Database	No. of record used	Total peaks	Assessment parameters
Sharma and Sharma, 2017 [120]	Band-pass filter + differentiation + weighted total variation denoising + low-pass filter	R peak	MIT-BIH European ST-T Fantasia	48 20 20	109,494 92,403 82,835	Se = 99.90%, + P = 99.88%, Er = 0.23% Se = 99.82%, + P = 99.63%, Er = 0.56% Se = 99.95%, + P = 99.73%, Er = 0.32%
Saadi et al., 2015 [133]	Band-pass filter + absolute value + smoothing + dual adaptive thresholds	QRS complex	Real time implementation MIT-BIH EDB eTDB eVDB	1 48 90 120 61	NR 91,285 759,878 45,248 38,429	Se = 99.86%, + P = 99.85%, Er = 0.29% Se = 99.90%, + P = 99.87% Se = 99.84%, + P = 99.71% Se = 99.88%, + P = 99.37% Se = 99.91%, + P = 99.79%
Kim and Shin, 2016 [134]	Band-pass filter + squaring + differentiation + moving average filter + adaptive threshold	QRS complex	MIT-BIH AHA	48 135	435,700	Se = 99.90%, + P = 99.91% Se = 99.84%, + P = 99.84%
Yakut and Bolat, 2018 [135]	Band-pass filter + squaring + moving average + normalization + adaptive thresholding	R peak	MIT-BIH Fantasia NSTDB QT	48 40 12 82	109,494 283,747 25,590 86,741	Se = 99.83%, + P = 99.83% Se = 99.94%, + P = 99.98% Se = 93.62%, + P = 94.52% Se = 99.89%, + P = 99.96%
Pan and Tompkins, 1985 [13]	Band-pass filter + differentiation + squaring + integration + dual thresholding	QRS complex	European ST-T MIT-BIH	90 48	790,565 116,137	Se = 99.61%, + P = 99.83% Dr = 99.3%, Er = 0.675%
Ferdi et al., 2003 [136]	Band-pass filter + non-linear transform and smoothing + adaptive threshold detection	R peak	MIT-BIH	48	109,492	Er = 0.37%
Benmalek and Charef, 2009 [137]	Fractional order band-pass filter + differentiation + squaring + smoothing + differentiation	R peak	MIT-BIH	47	107,632	Se = 99.86%, + P = 99.86%, Er = 0.28%, QDR = 99.86%
Nayak et al., 2018 [138]	Band-pass filter + digital first order differentiator + Hilbert transform + zero crossing detector	R peak	MIT-BIH	48	109,494	Se = 99.93%, + P = 99.92%, Er = 0.1507%, QDR = 99.92%

Table 3 (continued)

Authors	Technique used to design the algorithm	Feature detected	Database	No. of record used	Total peaks	Assessment parameters
Nayak et al., 2019 [139]	Band-pass filter + gases Brownian motion optimization based digital differentiator + Hilbert Transform + zero crossing detector	R peak	MIT-BIH	48	109,494	Se = 99.92%, + P = 99.92%, Da = 99.84%, Er = 0.1562%, QDR = 99.92%, Fs = 0.9992%
Bashar et al., 2019 [140]	Band-pass filter + variable frequency complex decomposition method (VFCDM) for ECG reconstruction and beat detection + dynamic amplitude thresholding	R peak	MIT-BIH UMass DB MIMIC III	48 22(subject) 20(subject)	109,457 10,216 17,809	Se = 99.94%, + P = 99.95%, Er = 0.11% Se = 99.95%, + P = 99.89%, Er = 0.16% Se = 100%, + P = 99.96%, Er = 0.04%
Chin et al., 2019 [141]	Band-pass filter + variance-based detection + maximum-likelihood estimation	Onset, period, and duration of QRS	Saltwater ECG data set MIT-BIH	NR 48	1258 109,357	Se = 99.75%, + P = 99.75%, Er = 0.50% Se = 99.86%, + P = 99.85%, Er = 0.29%
Nayak et al., 2019 [142]	Band-pass filter + digital fractional order differentiator + Shannon energy calculation + Hilbert transform + zero crossing detector	R peak	QTDB MIT-BIH STDB SVDB EDB QTDB TWADB	NR 48 28 78 90 82 100	NR 109,494 76,175 184,582 790,560 86,995 18,993	Se = 99.96%, + P = 99.94%, Er = 0.10% Se = 99.95%, + P = 99.94%, Er = 0.11% Se = 99.94%, + P = 99.92%, Er = 0.14% Se = 99.91%, + P = 99.90%, Er = 0.18% Se = 99.87%, + P = 99.86%, Er = 0.27% Se = 99.95%, + P = 99.98%, Er = 0.06% Se = 99.43%, + P = 99.25%, Er = 1.32%

**Table 3** (continued)

Authors	Technique used to design the algorithm	Feature detected	Database	No. of record used	Total peaks	Assessment parameters
Nayak et al., 2019 [143]	Band-pass filter + gravitational search algorithm based Integer order digital differentiator + smooth envelope extractor + non-amplitude threshold R-peak detection logic	R peak	MIT-BIH	48	109,494	Se=99.92%, +P=99.92%, Er=0.15%, QDR=99.92%, Da=99.84%, Fs=0.9992
			QTDB	105	111,134	Se=99.98%, +P=99.96%, Er=0.07%, QDR=99.96%, Da=99.93%, Fs=0.9997
			NSTDB	12	25,590	Se=95.23%, +P=94.41%, Er=10.41%, QDR=94.41%, Da=90.15%, Fs=0.9482
			AFTDB	60	7592	Se=99.03%, +P=99.76%, Er=1.21%, QDR=99.03%, Da=98.79%, Fs=99.39
			STDB	28	76,175	Se=99.93%, +P=99.90%, Er=0.17%, QDR=99.90%, Da=99.83%, Fs=0.9992
Rivas et al., 2015 [121]	Derivative + integral + squaring + thresholding	R peak	MIT-BIH	48	109,949	Se=99.543%, +P=99.737%
			NSRDB	NR	192,389	Se=99.967%, +P=99.991%
			ADB	NR	197,009	Se=99.452%, +P=99.322%
			Apnea ECG	NR	703,750	Se=99.901%, +P=99.771%
			Fantasia	NR	19,445	Se=99.989%, +P=99.940%
			Challenge 2014	NR	72,309	Se=99.935%, +P=99.753%
Kumar et al., 2019 [88]	Fast Fourier transform based band-pass filter	R peak	MIT-BIH	48	NR	Se=99.65%, +P=99.65%, Er=0.6% (Short length)
						Se=99.98%, +P=99.96%, Er=0.03% (full length)
Xie et al., 2019 [96]	Band-pass filter + discrete short-time Fourier transform + convolutional neural network	N, S, V, F and Q beat	MIT-BIH	44	NR	Se=75.6%, +P=90.1%, Da=98.4%, Sp=99.5%, Fs=0.82 (S beat)
Shaik et al., 2015 [94]	Low-pass filter + short time Fourier transform + adaptive thresholding	QRS peak	MIT-BIH	48	109,011	Se=99.56%, Sp=99.52%, Er=0.93%
Yazdani and Vesin, 2016 [144]	Low-pass filter + mathematical morphology filtering with a structuring element	QRS complex and other fiducial points	MIT-BIH	48	109,494	Se=99.87%, +P=99.9%, Er=0.2238

Table 3 (continued)

Authors	Technique used to design the algorithm	Feature detected	Database	No. of record used	Total peaks	Assessment parameters
Jain et al., 2016 [145]	Detrending + linear decreasing inertia—particle swarm optimization based adaptive filter + adaptive thresholding	QRS complex	MIT-BIH	48	109,494	Se = 99.75%, + P = 99.83%, Er = 0.42%
Pandit et al., 2017 [146]	Moving average filter + dynamic thresholding + max-min difference generation	R peak	MIT-BIH EDB STDB INCA RTDB QTDB	48 NR NR NR NR	109,809 790,495 70,755 174,644 86,435	Se = 99.62%, + P = 99.67%
Christov, 2004 [122]	Moving average filter + combined adaptive thresholds	QRS complex	MIT-BIH	48	110,050	Se = 99.69%, Sp = 99.66% (algorithm I) Se = 99.74%, Sp = 99.65% (algorithm-II)
Lee et al., 2018 [147]	Median filter + signal envelope filtering + Shannon energy + Savitzky-Golay filter	R peak	Normal ECG in physical activity (NPADB)	23 (sit) 23 (walk) 23 (ascend)	8385 10,775 14,048	Se = 99.99%, + P = 99.99%, Er = 0.03% Se = 99.93%, + P = 99.52%, Er = 0.55% Se = 99.94%, + P = 99.82%, Er = 0.24%
			QTDB	82	86,892	Se = 99.96% ( $\pm 0.08$ ), + P = 99.96% ( $\pm 0.11$ ), Er = 0.08% ( $\pm 0.14$ )
			NSTDB	2	4265	Se = 90.20% ( $\pm 0.45$ ), + P = 87.73% ( $\pm 2.06$ ), Er = 22.43% ( $\pm 2.79$ ) (0 dB SNR)
Sharma and Sunkaria, 2016 [148]	Median filter + Savitzky-Golay filter + baseline identification + thresholding	QRS complex	MIT-BIH Fantasia NSTDB	48 22 11	109,488 160,844 113,138	Se = 99.50%, + P = 99.56%, Er = 0.93%, Da = 99.08% Se = 99.90%, + P = 99.91%, Er = 0.19%, Da = 99.81% Se = 99.36%, + P = 99.43%, Er = 1.21%, Da = 98.81%
			BIDMC congestive heart failure Self-recorded dataset	5 15	61,682 15,164	Se = 99.68%, + P = 99.78%, Er = 0.52%, Da = 99.46% Se = 99.97%, + P = 99.99%, Er = 0.04%, Da = 99.96%
Rufas and Carrabina, 2015 [123]	MaMeMi filter + triangular detector + adaptive threshold detection	QRS complex	MIT-BIH	48	109,494	Se = 99.43%, + P = 99.67%, DR = 99.22%, Er = 0.88%



**Table 3** (continued)

Authors	Technique used to design the algorithm	Feature detected	Database	No. of record used	Total peaks	Assessment parameters
Jain et al., 2016 [149]	Mean subtraction + adaptive linear predictor + Savitzky-Golay filter + squaring and moving averaging filtering + adaptive thresholding	QRS complex peak	MIT-BIH	48	3706	Se = 99.68%, + P = 99.84%
Elgendi et al 2017 [150]	Sampling rate conversion + TERMA algorithm (Filtering + enhancing + potential block generation + thresholding)	QRS complex	MIT-BIH QTDB	48 105	109,985 111,201	Se = 99.78%, + P = 99.92% Se = 99.90%, + P = 99.84%
Zidelmal et al 2014 [151]	S transform and Shannon energy	R peak	MIT-BIH	48	108,494	Se = 99.84%, + P = 99.91%, Er = 0.25%
Birendra Biswal, 2017 [152]	Median filter + band-pass filter + modified S- transform with an amplitude threshold	R peak	MIT-BIH	48	108,494	Se = 99.91%, + P = 99.91%, Da = 99.77%
Chen and Chuang, 2017 [153]	Refreshment of ECG + signal enhancement + QRS fiducial point detection + recognition of R point on template matching	R peak	MIT-BIH	48	109,443	Se = 99.82%, + P = 99.81%, Er = 0.36%
Yochum et al., 2016 [105]	Continuous wavelet transform	QRS complex, T and P- wave	Computers in Challenge 2011 database	50	NR	Se = 99.87%, + P = 91.75%, Ac = 98.64%, Sp = 98.42%, Y <sub>w</sub> = 98.29%
Li et al., 1995 [103]	Wavelet transform	R peak, QRS onset and offset, T and P-wave	MIT-BIH	48	109,491	Se = 99.85%, + P = 99.48%, Er = 0.67%
Merah et al., 2015 [154]	Stationary wavelet transform	R peak	MIT-BIH	46	116,137	Er = 0.15%, DR > 99.8%
Banerjee et al., 2012 [100]	Discrete wavelet transform + QRS complex window finding by thresholding	R peak	MIT-BIH	48	109,494	Se = 99.84%, + P = 99.88%, Er = 0.28%
Berwal et al., 2018 [155]	Biorthogonal spline wavelet transform + threshold	QRS complex peak	QTDB NSTDB MIT-BIH	105 12 NR	86,892 25,590 19,098	Se = 99.94%, + P = 99.89%, Er = 0.18% Se = 95.30%, + P = 93.98%, Er = 10.81% Se = 99.6%, + P = 99.5%
		QRS complex peak	MIT-BIH, NSTDB, and MIT-BIH atrial fibrillation	43	3208	Se = 99.31%, + P = 99.19%, Er = 1.49%

Table 3 (continued)

Authors	Technique used to design the algorithm	Feature detected	Database	No. of record used	Total peaks	Assessment parameters
Sabherwal et al., 2018 [106]	Discrete wavelet transform + digital filter + adaptive thresholding + fusion algorithm	S peak and R peak	MIT-BIH	48	109,498	Se = 99.99%, + P = 99.99%, Da = 99.98%, Er = 0.135%, MSE = 0.039
Li et al., 2017 [104]	Wavelet transform + modulus maxima pair identification + R position modification	R peak	MIT-BIH	48	109,478	Se = 99.60%, + P = 99.77%
Rekik and Ellouze, 2016 [124]	Entropy criterion + wavelet transform modulus maxima	R peak	QTDB	11	86,995	Se = 99.94%, + P = 99.99%
Sharma et al., 2019 [156]	Tunable Q wavelet transform and correntropy based envelop extraction	R peak	MIT-BIH	48	109,494	Se = 99.89%, + P = 99.83%, Er = 0.29%
Sabherwal et al., 2017 [98]	Wavelet transform + first and second derivative and Hilbert transform	R peak	MIT-BIH QTDB NSTDB	48 NR NR	109,494 NR NR	Se = 99.9%, + P = 99.9%, Da = 99.8%, Er = 0.2% (Avg.)
Sahoo et al., 2016 [99]	Wavelet transform + differentiation + Hilbert transform with adaptive threshold	R peak	MIT-BIH	19	44,329	Se = 99.71%, + P = 99.72%, Er = 0.52%
Rakshit and Das, 2017 [101]	Wavelet transform + Shannon energy calculation and Hilbert transform	R peak	MIT-BIH	48	109,410	Se = 99.93%, + P = 99.91%, Da = 99.83%, Er = 0.17%, Fs = 0.9992
Park et al., 2017 [102]	Wavelet transform + Shannon energy envelope + peak energy envelope	R peak	MIT-BIH	48	109,494	Se = 99.93%, + P = 99.91%, Da = 99.838%, Er = 0.163%
Farashi, 2016 [125]	undecimated wavelet transform + multi-resolution time dependent entropy + thresholding	QRS complex peak	MIT-BIH	48	109,965	Se = 99.75%, + P = 99.85%, Er = 0.396
Ravanshad et al., 2014 [157]	asynchronous level-crossing analog-to-digital converter and nonuniformly spaced data processing	QRS complex	CSE	NR	NR	DR = 99.82%
Qin et al., 2017 [158]	Wavelet based multi resolution analysis + adaptive thresholding	R peak	MIT-BIH QTDB	48 82	109,428 86,995	Se = 98.89%, + P = 99.40%, Er = 1.71% Se = 99.39%, + P = 99.49%, Da = 98.89% Se = 99.83%, + P = 99.90%, Da = 99.73%

**Table 3** (continued)

Authors	Technique used to design the algorithm	Feature detected	Database	No. of record used	Total peaks	Assessment parameters
Deeptu and Lian, 2015 [159]	Adaptive sign-sign least mean square predictor + Savitzky-Golay filter + squaring and sum + adaptive thresholding	R peak	MIT-BIH	48	109,508	Se = 99.64%, + P = 99.81%
Tang et al., 2018 [160]	Parallel delta modulator + local maximum point and local minimum point algorithms	QRS complex, P, and T wave	MIT-BIH	48	109,966	Se = 99.17%, + P = 99.55%, Er = 1.28%
			QTDB	103	3129 (P peak)	Se = 91.12%, + P = 92.44%
					3475 (T peak)	Se = 98.36%, + P = 98.99%
Hou et al., 2018 [126]	Phase portraits and box scoring algorithm	QRS complex	MIT-BIH	48	110,008	Se = 99.32%, + P = 99.45%
Li et al., 2018 [161]	Phase space reconstruction	R peak	Experimental result	23	1890	Se = 96.55%, + P = 97.53%
			MIT-BIH	48	109,494	Se = 99.87%, + P = 99.93%, Da = 99.81%
			NSTDB	24	51,180	Se = 99.56%, + P = 93.05%, Da = 92.67%
			Long term ST	86	8,897,780	Se = 99.87%, + P = 99.96%, Da = 99.91%
Bajaj and Kumar, 2019 [162]	Fractional Stockwell transform and fractional Stockwell Shannon energy	R peak	MIT-BIH	48	109,494	Se = 99.99%, + P = 99.97%, Er = 0.03%, Da = 99.97%
Hossain et al., 2019 [163]	Moving window median filter + complete ensemble empirical mode decomposition with adaptive noise approach	QRS complex and P-wave	MIT-BIH	48	109,441	Se = 99.97%, + P = 99.93%, Er = 0.11%
			QTDB	80	86,989	Se = 99.96%, + P = 99.89%, Er = 0.15%
			NSTDB	NR	4268	Se = 99.25%, + P = 90.05%
Gupta et al., 2019 [118]	Independent principal component analysis + chaos analysis and principal component analysis	R peak	MIT-BIH	36	101,275	Se = 99.95%, + P = 99.96%, Er = 0.093%
			Ventricular tachyarrhythmia challenge	02		
			Atrial fibrillation termination challenge	04		
			AHA	02		
			MIT-BIH long-term	04		
			Real time dataset	7	16,501	Se = 99.96%, + P = 99.97%, Er = 0.055%

Table 3 (continued)

Authors	Technique used to design the algorithm	Feature detected	Database	No. of record used	Total peaks	Assessment parameters
Jia et al., 2020 [164]	High-resolution wavelet packet decomposition + convolutional neural network	QRS complex	Telehealth	NR	NR	Se = 98.99%, + P = 95.57%, Er = 5.61%, Fs = 97.25%
			NSTDB	NR	NR	Se = 99.25%, + P = 96.31%, Er = 4.55%, Fs = 97.76%
			MIT-BIH	NR	NR	Se = 99.89%, + P = 99.90%, Er = 0.21%, Fs = 99.89%
Chen and Maharatna, 2020 [165]	High-pass filter + low-pass filter + hierarchical clustering + discrete wavelet transform	R peak and T peak	MIT-BIH	48	NR	Se = 99.89%, + P = 99.94%, Da = 99.83%
			QTDB	103	NR	Se = 100%, + P = 99.83%, Da = 99.83% (for R peak)
						Se = 99.91%, + P = 99.38%, Da = NR (for T peak)
Modak et al., 2021 [127]	Median filter + moving average filter + segmentation and statistical false peak elimination	QRS complex	MIT-BIH	48	109,494	Se = 99.82%, + P = 99.88%, Er = 0.31%
			Fantasia	40	285,308	Se = 99.92%, + P = 99.90%, Er = 0.18%
Fotoohinasab et al., 2021 [166]	graph-constrained change-point detection	QRS complex	MIT-BIH	NR	NR	Se = 99.64%, + P = 99.71%, Er = 0.19 (manually defined constraint graph)
						Se = 99.76%, + P = 99.68%, Er = 0.55 (automatic learning constraint graph)
Morshedlou et al. 2021 [128]	Differentiation + square + low-pass filter	QRS complex	MIT-BIH	48	109,428	Se = 99.20%, + P = 99.40%, Er = 1.46%
			NSTDB	12	NR	Se = 99.94%, + P = 99.80%, (For record-11924 at 24 dB SNR)
			BIDMC congestive heart failure	15	93,092	Se = 98.70%, + P = 99.40%, Er = 1.88%

\*NR not reported, Se sensitivity, + P positive predictivity, Er error rate, Da detection accuracy, DR detection rate, QDR QRS detection rate

biological neural network. The virtues of ANNs, like learning complex, non-linear surfaces among different classes, make them suitable for ECG beat detection and classification [169]. Multilayer perceptron, self-organizing feature map (SOFM) learning vector quantization, and radial basis function networks are used to process an ECG signal. Xie et al. [96] proposed a convolution neural network (CNN) for the classification and achieved a detection accuracy of 98.4%. Kohler et al. [170] proposed zero-crossing detection of QRS complexes. In zero-crossing detection, a feature is obtained by counting the number of zero crossings per segment. The zero-crossing feature primarily does affect the sudden amplitude changes in the ECG signal, thus providing robustness to noise. The amplitude fluctuations in the problematic sections of an ECG signal do not affect the count of zero-crossing, which significantly improves detection performance. The zero-crossing detection method has the advantage of simplicity and low computational costs.

In [144], mathematical morphology (MM) is proposed to extract the QRS fiducial point. MM is used to extract the topological information from the analysis of the geometrical structure. MM operator non-linearly transforms the signal into another signal called the structuring element (SE). SE is used to detect QRS complexes. The R peak detection using zero-crossing detection concepts was reported in [138, 139, 142]. In [138, 139, 142], the properties of Hilbert transform and zero-crossing locations are used to detect an R peak. The odd symmetry property of an HT provides a zero at each maximum, thus providing a zero whenever the input signal crosses the zero axes. These zero crossing locations are used to locate the true position of an R peak. Li et al. [161] proposed a QRS complex detection method by coordinate mapping based on the phase space reconstruction. Tang et al. [160] employed a delta modulator along with local maximum point (LMaP) and local minimum point (LMiP) algorithm to detect QRS complex, P, and T wave. Different researchers have proposed various QRS and R peak detection techniques, but no technique has provided 100% accuracy with all the standard datasets with all records. Also, their clinical implementation is doubtful.

Another important parameter, which affects the performance of the available QRS complex detection algorithms, is the sampling rate and sampling resolution of the selected ECG data. Sampling is a process of converting a continuous-time signal into a discrete-time signal. According to the Nyquist theorem [171], the sampling frequency must be greater than or equal to twice the signal's maximum frequency to be digitized. If the sampling rate is low, the high-frequency components superimpose low-frequency components, introducing an error into the reconstructed signal. It is required to choose proper sampling frequency so that the accuracy of the QRS complex detection algorithms is not affected [172]. The maximum heartbeat is at most 220

beats per minute (bpm), corresponding to a frequency of less than 4 Hz. In an ECG signal, the spectrum of heartbeat signals extends up to 15 Hz, and some features extend beyond 25 Hz. Hence as per the Nyquist criterion, a minimum sampling frequency of 50 Hz is required. However, in real ECG recorders, the sampling frequencies range from 100–500 Hz, whereas in a lab environment, the sampling frequencies go up to 1000 Hz [172]. In 1975, a minimum sampling rate of 500 Hz, with uniform sampling, generally two or three times of theoretical minimum sampling rate, is recommended by the American Heart Association (AHA) [173]. According to the AHA task force [174], a low sampling rate may yield a jitter in R peak detection, significantly altering the spectrum. The optimal range of sampling frequency for R peak detection is 250–500 Hz or more. The sampling resolution (or bit depth) is another factor that affects the accuracy of heartbeat detection [172]. Sampling resolution produces a signal to quantization noise ratio, which results in an error in the beat detection. Ajaraga et al. [172] showed that 8-bit or lower sampling resolution is unacceptable for QRS complex detection, especially at high sampling frequencies. The frequency resolution of 10-bit shows acceptable results, but an accurate analysis requires a 12-bit resolution [172].

## 5 Databases

The ECG databases play a significant role in the development of any algorithm related to ECG signal analytics. These databases provide a wide range of annotated ECG signals recorded under different conditions. Depending on the application, various researchers use various databases to evaluate the performance of the proposed ECG signal analysis algorithms. Details on some important databases are available in [175]. Table 4 summarizes these databases, along with their salient features.

- (a) *Massachusetts Institute of Technology-Beth Israel Hospital Arrhythmia database (MIT-BIH)* is a popular database that consists of 48 half-hour ECG recordings from two channels. The ECG signals are from 47 subjects recorded at Boston's Beth Israel Hospital between 1975 to 1979. Of 47 subjects, 25 subjects were men, aged 32 to 89, and 22 subjects were women, aged 23 to 89. Of these recordings, 60% of records are from inpatients, and 40% are from outpatients. The sampling frequency is 360 samples per second, facilitating 60 Hz notch filters [24–26, 138].
- (b) *The American Heart Association database (AHA)*- The American heart association, along with funding agency National Heart, Lung, and Blood Institute (NHLBI), motivated the development of a new ECG database at Washington University, which is known as the AHA

**Table 4** Overview of various databases used in ECG signal processing

Sr. no.	Database	Subjects	Number of records	Length of record (minutes)	Number of lead	Sampling frequency	Bit Resolution (bits per sample)	References	Availability
1	The American Heart Association (AHA)	N/A	80	35	2	250 Hz	12	[178]	Open access
2	Creighton University (CU) Ventricular Tachyarrhythmia	N/A	35	8	1	250 Hz	12	[179]	Open access
3	QT database	N/A	105	15	2	250 Hz	N/A	[180]	Open access
4	Non-Invasive Fetal ECG	1	55	Variable duration	multiple	1 kHz	16	[181]	Open access
5	Apnea-ECG	NA	70	401–578		100 Hz	16	[182]	Open access
6	Fetal ECG Synthetic	10	1750	5	34	250 Hz	16	[183]	Open access
7	St Petersburg INCART 12-lead Arrhythmia	32	75	30	12	257 Hz	NA		Open access
8	Fantasia	40	40	120	NA	250 Hz	NA	[184]	Open access
9	BIDMC Congestive Heart Failure	15	15	1200	12	250 Hz	NA	[185]	Open access
10	MIT-BIH ST Change	28	28	13–67	1–2	360 Hz	NA	[186]	Open access
11	MIT-BIH Normal Sinus Rhythm	18 (5 Men + 13 Women)	18	1440	2	128 Hz	NA		Open access
12	MIT-BIH Arrhythmia	47	48	30	2	360 Hz	11	[187]	Open access
13	MIT-BIH Atrial Fibrillation	25	25	600	2	250 Hz	12	[188]	Open access
14	European ST-T	79	90	120	2	250 Hz	12	[189]	Open access
15	PTB	290	549	N/A	12 (conventional) + 3 (Frank)	1000 Hz	16	[190]	Open access

database. This database includes 80 two-channel recordings. A sampling frequency of 250 Hz per channel over the ten mV range with the 12-bit resolution is used for digitalization. This database is available in two versions: a short version and a long version. The short version consists of an unannotated recording of 5 min before 30 min annotated ECG recording. In the long version, 2.5 h of unannotated recording is present before each annotated part [118, 134, 176, 177].

(c) *Creighton University (CU) Ventricular Tachyarrhythmia database* consists of 35 eight-minute ECG recordings of subjects suffering from Ventricular tachycardia, ventricular flutter, and Ventricular fibrillation. All

records are digitized at a sampling rate of 250 Hz with a 12-bit resolution over the ten mV range [176, 177].

(d) *BIDMC Congestive Heart failure database*—It includes long-term ECG records from 15 subjects. Out of 15, 11 are men aged between 22 and 71 years, and the remaining are women aged between 54 and 63 years. All records are digitized at a sampling rate of 250 Hz with a 12-bit resolution over the  $\pm 10$  mV range [40, 149].

(e) *QT database*—This database is a collection of various ECG recordings collected from existing databases. The QT database consists of *thirteen* records from the MIT-BIH Supraventricular Arrhythmia database, fifteen records from the MIT-BIH Arrhythmia data-

base, *thirty-three* from the European ST-T database, *six* records from the MIT-BIH ST change database, *ten* records from the MIT-BIH normal sinus rhythm arrhythmia database, four from MIT-BIH long term database and twenty-four records were from sudden death patients at Boston’s Beth Israel Deaconess Medical center. In total, the database covers 105 records, two-channel recordings to avoid baseline fluctuations or other artifacts [135, 141, 147, 156, 158, 160, 163].

- (f) *European ST-T Database*—Ninety annotated ECG records from seventy-seven subjects are present in this database. Seventy subjects were men of age group 30 to 84 years, and eight subjects are women age 55 to 71. Each record consists of two signals of 2 h duration. A sampling frequency of 250 samples per second with a 12-bit resolution over the input range of 20 mV [120, 135] is used for digitizing the signals.
- (g) *Fantasia Database* consists of forty ECG recordings, twenty records from the young population age 21 to 34 years, and twenty from the elderly aged population aged 68 to 85 years. All the recording is 120 min duration long. The ECG signals are recorded when the subjects are at rest and watching a Fantasia movie. The sampling rate for digitalization is 250 Hz [41, 120, 121, 135].
- (h) *PTB Diagnostic Database*—This database is a collection of 549 ECG records from 290 subjects. The database contains ECG recordings of 209 men with a mean age of 55.5 years and 81 women with a mean age of 61.6 years. Signals are sampled with a sampling frequency of 1000 Hz. Resolution is 16 bits over a range of  $\pm 16.384$  mV [40, 43, 45].
- (i) *Long Term ST Database*—This database includes 86 long-term ECG records from 80 subjects. The records are 21 to 24 h long, containing two to three ECG signals. The sampling frequency is 250 samples per second over the  $\pm 10$  mV range with 12-bit resolution [47, 161].
- (j) *Non-Invasive Fetal ECG Arrhythmia Database (NIFEADB)* consists of 55 recordings taken from a single pregnant subject recorded over twenty weeks.
- (k) *ECG ID Database*—It includes 310 recordings taken from 90 subjects. *Forty-four* men and *46* women from different fields (students, colleagues, and friends of the author) are taken for the recording. The ECG signal sampling frequency is 500 Hz with a 12-bit resolution over  $\pm 10$  mV [37].
- (l) *St Petersburg Institute of Cardiological Technics (INCART) Database* includes 75 annotated recordings. The duration of each record is 30 min long and covers 12 standard leads. Seventeen men and 15 women aged between 18 to 80 years are selected for recording. The sampling rate for each ECG record is 257 Hz [146].

- (m) *Apnea-ECG database*—It is a dataset of 70 records. The length of these records may vary from less than 7 h to 10 h. Each recording includes three facts: a continuous digitized ECG signal, apnea annotation, and machine-generated QRS annotation. These seventy recordings are divided into a learning set and a test set of 35 recordings [39, 121].

## 6 Parameters to Evaluate the Performance of an ECG Algorithm

Various parameters are used in the literature to evaluate the ECG algorithms proposed by various researchers. These success measures are an integral part of ECG signal analysis. Evaluation parameters not only evaluate the algorithms but also provides a medium for comparison of various proposed algorithms. Different evaluation parameters are presented in this section. In the following equations,  $S(n)$ ,  $X(n)$ ,  $X'(n)$ , and  $Y(n)$  represents a corrupted signal, original signal, pre-processed signal, and denoised signal, respectively.  $N$  is the length of the ECG signal.

the Input signal to noise ratio,  $SNR_{input}$

$$= 10 \log_{10} \left( \frac{\sum_{n=1}^N (X'[n])^2}{\sum_{n=1}^N (S[n])^2} \right) \tag{2}$$

(i)

Output signal to noise ratio,  $SNR_{out}$

$$= 10 \log_{10} \left( \frac{\sum_{n=1}^N Y^2[n]}{\sum_{n=1}^N (X[n] - Y[n])^2} \right) \tag{3}$$

(ii)

Improvement in signal to noise ratio,  $SNR_{imp}$

$$= SNR_{out} - SNR_{input} \tag{4}$$

$$= 10 \log_{10} \left( \frac{\sum_{n=1}^N (S[n] - X[n])^2}{\sum_{n=1}^N (Y[n] - X[n])^2} \right) \tag{4}$$

(iii)

Mean square error =  $MSE = \frac{1}{N} \sum_{n=1}^N (X[n] - Y[n])^2$

(iv)  $\tag{5}$

Percentage root mean square difference

$$= PRD = \sqrt{\frac{\sum_{n=1}^N (X[n] - Y[n])^2}{\sum_{n=1}^N X^2[n]}} \tag{6}$$

(v)

$$(vi) \quad \text{Sensitivity}(Se) = \frac{(\text{True Positive})}{(\text{True Positive} + \text{True Negative})} \quad (7)$$

$$(vii) \quad \text{Specificity}(Sp) = \frac{(\text{True negative})}{(\text{True Positive} + \text{False Positive})} \quad (8)$$

$$(viii) \quad \begin{aligned} \text{Positive predictivity}(+P) \\ = \frac{(\text{True positive})}{(\text{True Positive} + \text{False Positive})} \end{aligned} \quad (9)$$

$$(ix) \quad \text{Accuracy}(Ac) = \frac{(\text{True Positive} + \text{True negative})}{(\text{True Positive} + \text{True negative} + \text{False Positive} + \text{False Negative})} \quad (10)$$

$$(x) \quad \text{Detection Accuracy}(Da) = \frac{(\text{True Positive})}{(\text{True Positive} + \text{False Positive} + \text{False Negative})} \quad (11)$$

$$(xi) \quad \text{Error Rate}(Er) = \frac{(\text{False Positive} + \text{False Negative})}{\text{Total beat}} \quad (12)$$

$$(xii) \quad \begin{aligned} \text{QRS Detection Rate}(QDR) \\ = \text{Min}(\text{sensitivity}, \text{positive predictivity}) \end{aligned} \quad (13)$$

$$(xiii) \quad \text{F - score}(Fs) = \frac{(2 \times \text{Sensitivity} \times \text{positive predictivity})}{(\text{Sensitivity} + \text{positive predictivity})} \quad (14)$$

$$(xiv) \quad \text{Youden index}(Y_w) = Se + Sp - 1 \quad (15)$$

*True positive* represents the number of true QRS complexes that are correctly detected. *False-negative* is the number of QRS complexes that are not detected as a QRS complex. *False-positive* is the number of non QRS complexes that are detected as QRS complexes. *Sensitivity* represents the percentage of true beats that an algorithm can correctly detect. *Positive predictivity* is the percentage of detected beats that were true beats. *Accuracy* represents the ratio of correctly detected beats to the total number of beats. *QRS detection rate* is defined as sensitivity or positive predictivity, whichever is minimum.

## 7 Discussion and Challenges

Detection of cardiovascular diseases requires the accurate and precise detection of QRS complex detection. As the ECG signals suffer from various noises and artifacts, the pre-processing of the ECG signal is very necessary. The pre-processing step, which removes the noises and artifacts in the ECG signal analysis, directly influences the

outcome. This paper presents almost all of the existing ECG signal pre-processing techniques and QRS complexes detection techniques. The pre-processing methods, like filtering, transform, empirical, are used by different researchers. The study showed that a single technique is not enough to remove different kinds of artifacts and noises.

Moreover, each denoising technique produces some impact on the ECG signal. It is essential to identify the nature of noise first; after then, a denoising scheme should

be selected for those noises and artifacts [177]. In literature, hybrid techniques are used to improve the overall performance of the ECG detection algorithms. Hybrid techniques combine two techniques resulting in good denoising results at the cost of increased computation complexity and processing delay.

The presence of noises and artifacts in the ECG signal produces errors in QRS and R peak detection. Hence denoising step is a very crucial part of cardiovascular disease detection. Our survey showed that many proposed algorithms achieved good denoising results but with few ECG records. No single denoising scheme is validated with all the records of all the standard datasets. Among the various denoising techniques, the filtering technique is quite useful when the noise occurs in a known frequency range beyond the frequency range of the ECG signal. When the noise lies within the ECG signal's frequency range, the transform techniques such as DFT and DCT have shown good denoising performance without distorting the signal. Line fitting techniques such as Savitzky-Golay filtering may appear as a powerful tool when the frequency range of noise is unpredicted and widespread. Savitzky-Golay filtering can smooth the signal without destroying the original property of the ECG signal. Other transform techniques such as STFT, wavelet have also been used for denoising, but they are not suitable for long-term ECG signals.

Some decomposition techniques such as EMD, EEMD, VMD, Fourier decomposition methods are useful for specific noises such as baseline wander, power line interference, and electromyographic noise. These techniques are capable of removing some of the noises and artifacts present in the ECG signal. Further, the performance of



the algorithm is evaluated using few ECG records. Most of the denoising techniques have successfully overcome the BW and PLI noise, but removing other noises is still a challenging task. In several studies, beat averaging is used to remove noise, but its usefulness and effect on the specificity and sensitivity of detection algorithms require further studies.

Detection of the QRS complex or R peak depends on the quality of the ECG signal. In the presence of artifacts and noises, the detection accuracy may decrease, and the wrong identification of CVDs is possible. Hence, before detection, denoising is essential. Various methods are available in the literature for the detection of QRS complexes and R peak detection. Almost all the techniques utilize the pre-processing or denoising step before detection to improve the detection accuracy. Recent studies reported excellent detection accuracies by excluding the noisy record of the standard dataset. The detection accuracies of some of the proposed ECG detectors are very high when applied on a limited dataset and under specific conditions, and the algorithms are not validated over all the datasets. Further, very few proposed algorithms implemented in a real-time system suffered from low detection accuracies.

Although different researchers have proposed various QRS denoising and detection techniques, many are not tested against all standard databases, so it is difficult to compare and evaluate their results. Some proposed algorithms in the literature achieved high sensitivity and accuracy, but they have excluded the noisy record of the database. Therefore, these algorithms may not be useful for clinical purposes. Most detection techniques have used different pre-processing and detection methods, which results in complexity and time consumption. Still, no powerful technique is proposed in the literature that can be used for denoising and detection and provides good performance results. Although wavelet transform has been used for denoising and detection both, the performance is not very good. Also, the selection of mother wavelets in the wavelet transform is a difficult task. The practical implementation of the proposed algorithms is a big challenge in ECG signal analysis. Recent studies show that along with denoising and detection, the lossless data compression of the ECG signal is also essential. The lossless compression capability is necessary because it minimizes storage, transmission, and computational data. In literature, very few algorithms have compression capability.

Our studies reveal that the evaluation parameters like accuracy, sensitivity represent the overall performance of the algorithms. However, the portion of the algorithm accountable for the improvement in the evaluation parameters is not provided. The assessment of the algorithms based on

features is very important as it would help in the secondary analysis and explaining the cause of heart abnormalities. In the literature, the outcomes of the proposed algorithms are not compared with the ECG recorders' output, which medical professionals use. This comparison will help validate the proposed algorithms and demonstrate the efficacy of the proposed algorithm over the currently used methods by medical professionals. Most of the proposed algorithms are based on QRS complex detection or R-peak detection while ignoring other characteristics like the ST segment and P-wave. Nevertheless, clinically, these characteristics are equally important as QRS complex or R peak.

Most of the reviewed papers have been used different standard databases such as MIT-BIH, AHA, PTB. Although the records have a long duration and enough information in these databases, these records are obtained from a small number of subjects, which is clinically insignificant. Moreover, most proposed algorithms are validated over the same database, limiting the reliability and research findings. Also, labels and annotations of these standard database records are too old to define the new definitions of the CVDs with great reliability. Hence there is a demand for new databases, which are created with modern and precise devices. The annotation and label of this new database records must match with the recent guidelines for CVDs detection. For the advancement in technology, it is required to have an ECG database with many records to evaluate the statistical significance.

Another major issue in the analysis of the ECG signal is ignoring the background of the subject. Apart from patient age, no other information is used by the proposed algorithms. The subject's medical history, symptoms, and different signs were not included in the literature. However, the inclusion of this information in the proposed algorithms can significantly improve the performance. Nowadays, the wide availability of computing technology offers a significant improvement in ECG signal analysis. The increasing low-cost, high-performance computing technology can provide a reliable and appropriate automatic ECG signal diagnosis solution. Various machine learning algorithms are proposed in the literature to denoise and classify ECG signals. The number of training datasets limits the performance of these machine learning algorithms. Many training datasets are required to develop an accurate system, which in turn increases the system complexity. For early and accurate detection of CVDs, developing a technique that can effectively perform both denoising and detection is required. The technique must be capable of providing the characteristics information of the ECG signal. The technique should be practically implementable, cost-effective, non-invasive, and

low time-consuming. It must have compression capability to be easily used in portable and smart ECG detector devices.

## 8 Conclusions

CVDs possess a severe health risk worldwide, can be predicted by accurately analyzing ECG signals. This paper aims to consolidate the information on various existing algorithms to analyze an ECG signal. The performance of an algorithm depends on various other factors like noise and database, so a summary of noise and database is also discussed.

In literature, the problems associated with the techniques to analyze the ECG signal are discussed. The primary step in ECG signal analysis is the removal of various noises present in the ECG signal. Denoising is the most critical step in ECG signal processing because the denoising step directly influences the outcome of the detection process. Many researchers suggest various techniques for denoising by minimizing or removing the effect of noises. The techniques used for denoising are based on time, frequency, time–frequency, and sparsity domain. Some hybrid techniques, arrived by combining two different approaches, are also used to remove noise from an ECG signal. Each method has its benefits and drawbacks, which are discussed in this paper. These different techniques used for denoising are summarised and compiled in this paper. The results of these techniques for ECG signal denoising on different databases are also presented.

The CVDs can be detected by identifying the ECG signal's morphological features from a denoised ECG signal. In the literature, R peak and QRS complex are used to detect ECG signal characteristics. Before detection, almost all algorithms use denoising or noise removal techniques. Different techniques have been proposed for the detection of ECG characteristics. Various proposed detection techniques have achieved commendable ECG peak detection accuracies on the standard databases. These various detection techniques, along with their performance parameters, are tabulated in this paper.

The proposed techniques for denoising and detection are validated on the various standard databases by the researchers. Most of the standard ECG databases are discussed in this paper. Different success parameters to compare the ECG signal analysis techniques are discussed in this paper. Some of the existing techniques have shown promising results their hardware realization is questionable. Studies show that very few methods are implemented on the hardware. Also, the

modern health care system requires wearable devices for continuous monitoring of cardiac health. Only a few existing techniques are implemented in wearable devices with limited accuracy. Indeed, a computational technique that can be used to analyze the ECG signal with higher accuracy in all conditions is still a requirement.

## Declarations

**Conflict of interest** All Authors of this work declare no conflict of interest.

**Ethical approval** This article does not contain any studies with human participants or animals performed by any of the authors.

## References

1. [https://www.who.int/en/newsroom/factsheets/detail/cardiovascular-diseases-\(CVD\)](https://www.who.int/en/newsroom/factsheets/detail/cardiovascular-diseases-(CVD)). Accessed 7 May 2021
2. Li P, Wang Yu, He J, Lihua Wang Yu, Tian T-S, Li T, Li J-S (2016) High-performance personalized heartbeat classification model for long-term ECG signal. *IEEE Trans Biomed Eng* 64(1):78–86. <https://doi.org/10.1109/TBME.2016.2539421>
3. da Luz EJS, Schwartz WR, Cámara-Chávez G, Menotti D (2016) ECG-based heartbeat classification for arrhythmia detection: a survey. *Comput Methods Prog Biomed* 127:144–164. <https://doi.org/10.1016/CMPB.2015.12.008>
4. Goldberger AL, Goldberger E (1981) Clinical electrocardiography, a simplified approach. *Crit Care Med* 9(12):891–892
5. Sörnmo L, Laguna P (2005) Bioelectrical signal processing in cardiac and neurological applications. Academic Press, Cambridge
6. Biel L, Pettersson O, Philipson L, Wide P (2001) ECG analysis: a new approach in human identification. *IEEE Trans Instrum Meas* 50(3):808–812. <https://doi.org/10.1109/19.930458>
7. Li Z, Li X, Zhu Z, Zeng S, Wang Y, Wang Y, Li A (2019) Signal analysis of electrocardiogram and statistical evaluation of myocardial enzyme in the diagnosis and treatment of patients with pneumonia. *IEEE Access* 7:113751–113759. <https://doi.org/10.1109/ACCESS.2018.2889354>
8. Bailón R, Sörnmo L, Laguna P (2006) A robust method for ECG-based estimation of the respiratory frequency during stress testing. *IEEE Trans Biomed Eng* 53(7):1273–1285. <https://doi.org/10.1109/TBME.2006.871888>
9. [https://ecgwaves.com/reference-values-for-ecg-electrocardiography/\(last\)](https://ecgwaves.com/reference-values-for-ecg-electrocardiography/(last)). Accessed 7 May 2021
10. Kumar A, Ranganatham R, Kumar M, Komaragiri R (2020) Hardware emulation of a biorthogonal wavelet transform-based heart rate monitoring device. *IEEE Sens J* 21(4):5271–5281. <https://doi.org/10.1109/JSEN.2020.3034742>
11. Cromwell L, Weibell FJ, Pfeiffer EA (1980) Biomedical instrumentation and measurements, 2nd edn. Prentice-Hall Inc., New Jersey
12. Rajankar SO, Talbar SN (2019) An electrocardiogram signal compression techniques: a comprehensive review. *Analog Integr Circ Sig Process* 98(1):59–74. <https://doi.org/10.1007/s10470-018-1323-1>
13. Pan J, Tompkins WJ (1985) A real-time QRS detection algorithm. *IEEE Trans Biomed Eng* 3:230–236. <https://doi.org/10.1109/TBME.1985.325532>

14. Friesen GM, Jannett TC, Jadallah MA, Yates SL, Quint SR, Nagle HT (1990) A comparison of the noise sensitivity of nine QRS detection algorithms. *IEEE Trans Biomed Eng* 37(1):85–98. <https://doi.org/10.1109/10.43620>
15. Satija U, Ramkumar B, Manikandan MS (2018) A review of signal processing techniques for electrocardiogram signal quality assessment. *IEEE Rev Biomed Eng* 11:36–52. <https://doi.org/10.1109/RBME.2018.2810957>
16. Clifford GD, Azuaje F, Mcsharry P (2006) ECG statistics, noise, artifacts, and missing data. *Adv Methods Tools ECG Data Anal* 6:18
17. Kligfield P, Gettes LS, Bailey JJ, Childers R, Deal BJ, William Hancock E, Van Herpen G et al (2007) Recommendations for the standardization and interpretation of the electrocardiogram: part I: the electrocardiogram and its technology a scientific statement from the American heart association electrocardiography and arrhythmias committee, council on clinical cardiology; the American college of cardiology foundation; and the heart rhythm society endorsed by the international society for computerized electrocardiology. *J Am Coll Cardiol* 49(10):1109–1127. <https://doi.org/10.1016/JACC.2007.01.024>
18. Luo S, Johnston P (2010) A review of electrocardiogram filtering. *J Electrocardiol* 43(6):486–496. <https://doi.org/10.1016/JELECTROCARD.2010.07.007>
19. <https://www.analog.com/media/en/training-seminars/design-handbooks/Basic-Linear-Design/Chapter8.pdf>. Accessed 09 May 2021
20. Kumar A, Komaragiri R, Kumar M (2019) Design of efficient fractional operator for ECG signal detection in implantable cardiac pacemaker systems. *Int J Circuit Theory Appl* 47(9):1459–1476. <https://doi.org/10.1002/cta.2667>
21. Acharya UR, Krishnan SM, Spaan JAE, Suri JS (eds) (2007) *Advances in cardiac signal processing*. Springer, Berlin
22. Jagtap SK, Uplane MD (2013) Digital filter approach for ECG in signal processing. In: *Proceedings of international conference on advances in computing*. Springer, New Delhi, pp. 1075–1082
23. Wang K, Ma S, Feng J, Zhang W, Fan M, Zhao D (2012) Design of ECG signal acquisition system based on DSP. *Proc Eng* 29:3763–3767. <https://doi.org/10.1016/PROENG.2012.01.567>
24. Lee Y, Hwang D (2018) Periodicity-based nonlocal-means denoising method for electrocardiography in low SNR non-white noisy conditions. *Biomed Signal Process Control* 39:284–293. <https://doi.org/10.1016/BSPC.2017.08.006>
25. Wang X, Zhou Y, Shu M, Wang Y, Dong A (2019) ECG baseline wander correction and denoising based on sparsity. *IEEE Access* 7:31573–31585. <https://doi.org/10.1109/ACCESS.2019.2902616>
26. Wang J, Ye Y, Pan X, Gao X (2015) Parallel-type fractional zero-phase filtering for ECG signal denoising. *Biomed Signal Process Control* 18:36–41. <https://doi.org/10.1016/BSPC.2014.10.012>
27. Cuomo S, De Pietro G, Farina R, Galletti A, Sannino G (2016) A revised scheme for real time ecg signal denoising based on recursive filtering. *Biomed Signal Process Control* 27:134–144. <https://doi.org/10.1016/BSPC.2016.02.007>
28. Mourad N (2019) ECG denoising algorithm based on group sparsity and singular spectrum analysis. *Biomed Signal Process Control* 50:62–71. <https://doi.org/10.1016/BSPC.2019.01.018>
29. Cuomo S, De Pietro G, Farina R, Galletti A, Sannino G (2015) A novel O (n) numerical scheme for ECG signal denoising. In: *ICCS*, pp. 775–784
30. Panigrahy D, Sahu PK (2016) Extended Kalman smoother with differential evolution technique for denoising of ECG signal. *Australas Phys Eng Sci Med* 39(3):783–795. <https://doi.org/10.1007/s13246-016-0468-4>
31. Jenkal W, Latif R, Toumanari A, Dliou A, El Bcharri O, Maoulainine FMR (2016) An efficient algorithm of ECG signal denoising using the adaptive dual threshold filter and the discrete wavelet transform. *Biocybern Biomed Eng* 36(3):499–508. <https://doi.org/10.1016/BBE.2016.04.001>
32. Singh P, Pradhan G, Shahnawazuddin S (2017) Denoising of ECG signal by non-local estimation of approximation coefficients in DWT. *Biocybern Biomed Eng* 37(3):599–610. <https://doi.org/10.1016/BBE.2017.06.001>
33. Lin H-Y, Liang S-Y, Ho Y-L, Lin Y-H, Ma H-P (2014) Discrete-wavelet-transform-based noise removal and feature extraction for ECG signals. *Irbm* 35(6):351–361. <https://doi.org/10.1016/IRBM.2014.10.004>
34. Wang F, Ji Z (2014) Application of the dual-tree complex wavelet transform in biomedical signal denoising. *Bio-Med Mater Eng* 24(1):109–115
35. El Bcharri O, Latif R, Elmansouri K, Abenaou A, Jenkal W (2017) ECG signal performance de-noising assessment based on threshold tuning of dual-tree wavelet transform. *Biomed Eng Online* 16(1):26. <https://doi.org/10.1186/s12938-017-0315-1>
36. Zhang S, Gao J, Yang J, Yu S (2013) A Mallat based wavelet ECG de-noising algorithm. In: *Applied mechanics and materials*, vol. 263. Trans Tech Publications Ltd, Freienbach, pp. 2267–2270. <https://doi.org/10.4028/www.scientific.net/AMM.263-266.2267>
37. Peng Z, Wang G (2017) Study on optimal selection of wavelet vanishing moments for ECG denoising. *Sci Rep* 7(1):1–11. <https://doi.org/10.1038/s41598-017-04837-9>
38. Han G, Zhijun Xu (2016) Electrocardiogram signal denoising based on a new improved wavelet thresholding. *Rev Sci Instrum* 87(8):084303. <https://doi.org/10.1063/1.4960411>
39. Hong HE, Yonghong TAN (2018) A novel adaptive wavelet thresholding with identical correlation shrinkage function for ECG noise removal. *Chin J Electron* 27(3):507–513. <https://doi.org/10.1049/CJE.2018.02.006>
40. Kumar A, Komaragiri R, Kumar M (2018) Heart rate monitoring and therapeutic devices: a wavelet transform based approach for the modeling and classification of congestive heart failure. *ISA Trans* 79:239–250. <https://doi.org/10.1016/ISATRA.2018.05.003>
41. Kumar A, Komaragiri R, Kumar M (2018) Design of wavelet transform based electrocardiogram monitoring system. *ISA Trans* 80:381–398. <https://doi.org/10.1016/ISATRA.2018.08.003>
42. Smital L, Vitek M, Kozumplik J, Provaznik I (2012) Adaptive wavelet wiener filtering of ECG signals. *IEEE Trans Biomed Eng* 60(2):437–445. <https://doi.org/10.1109/TBME.2012.2228482>
43. Hao H, Wang H, Rehman NU, Chen L, Tian H (2017) An improved multivariate wavelet denoising method using subspace projection. *IEICE Trans Fundam Electron, Commun Comput Sci* 100(3):769–775. <https://doi.org/10.1587/TRANSFUNE100.A.769>
44. Kumar A, Komaragiri R, Kumar M (2019) Time–frequency localization using three-tap biorthogonal wavelet filter bank for electrocardiogram compressions. *Biomed Eng Lett* 9(3):407–411. <https://doi.org/10.1007/s13534-019-00117-9>
45. Yadav SK, Sinha R, Bora PK (2015) Electrocardiogram signal denoising using non-local wavelet transform domain filtering. *IET Signal Process* 9(1):88–96. <https://doi.org/10.1049/IET-SPR.2014.0005>
46. Tracey BH, Miller EL (2012) Nonlocal means denoising of ECG signals. *IEEE Trans Biomed Eng* 59(9):2383–2386. <https://doi.org/10.1109/TBME.2012.2208964>
47. Qian C, Honghong Su, Helong Yu (2019) Local means denoising of ECG signal. *Biomed Signal Process Control* 53:101571. <https://doi.org/10.1016/BSPC.2019.101571>
48. Anapagamani SA, Rajavel R (2016) Hardware implementation of ECG denoising system using TMS320C6713 DSP processor.

- Int J Biomed Eng Technol 21(1):95–108. <https://doi.org/10.1504/IJBET.2016.076735>
49. Jain S, Bajaj V, Kumar A (2017) Riemann Liouville fractional integral based empirical mode decomposition for ECG denoising. *IEEE J Biomed Health Inform* 22(4):1133–1139. <https://doi.org/10.1109/JBHI.2017.2753321>
  50. Kumar S, Panigrahy D, Sahu PK (2018) Denoising of electrocardiogram (ECG) signal by using empirical mode decomposition (EMD) with non-local mean (NLM) technique. *Biocybern Biomed Eng* 38(2):297–312. <https://doi.org/10.1016/BBE.2018.01.005>
  51. Rakshit M, Das S (2018) An efficient ECG denoising methodology using empirical mode decomposition and adaptive switching mean filter. *Biomed Signal Process Control* 40:140–148. <https://doi.org/10.1016/BSPC.2017.09.020>
  52. Kabir MDA, Shahnaz C (2012) Denoising of ECG signals based on noise reduction algorithms in EMD and wavelet domains. *Biomed Signal Process Control* 7(5):481–489. <https://doi.org/10.1016/BSPC.2011.11.003>
  53. Singh P, Shahnawazuddin S, Pradhan G (2018) An efficient ECG denoising technique based on non-local means estimation and modified empirical mode decomposition. *Circuits Syst Signal Process* 37(10):4527–4547. <https://doi.org/10.1007/s00034-018-0777-9>
  54. Jain S, Bajaj V, Kumar A (2018) Effective de-noising of ECG by optimised adaptive thresholding on noisy modes. *IET Sci Meas Technol* 12(5):640–644. <https://doi.org/10.1049/IET-SMT.2017.0203>
  55. Wang M, Zhou Z, Li Z, Zeng Y (2019) An adaptive denoising algorithm for chaotic signals based on improved empirical mode decomposition. *Circuits Syst Signal Process* 38(6):2471–2488. <https://doi.org/10.1007/s00034-018-0973-7>
  56. Das MK, Ari S (2013) Analysis of ECG signal denoising method based on S-transform. *Irbm* 34(6):362–370. <https://doi.org/10.1016/IRBM.2013.07.012>
  57. Singhal A, Singh P, Fatimah B, Pachori RB (2020) An efficient removal of power-line interference and baseline wander from ECG signals by employing Fourier decomposition technique. *Biomed Signal Process Control* 57:101741. <https://doi.org/10.1016/BSPC.2019.101741>
  58. Tan C, Zhang L, Hau-tieng Wu (2018) A novel blaschke unwinding adaptive-Fourier-decomposition-based signal compression algorithm with application on ECG signals. *IEEE J Biomed Health Inform* 23(2):672–682. <https://doi.org/10.1109/JBHI.2018.2817192>
  59. Sharma RR, Pachori RB (2018) Baseline wander and power line interference removal from ECG signals using eigenvalue decomposition. *Biomed Signal Process Control* 45:33–49. <https://doi.org/10.1016/BSPC.2018.05.002>
  60. Kumar A, Tomar H, Mehla VK, Komaragiri R, Kumar M (2021) Stationary wavelet transform based ECG signal denoising method. *ISA Trans* 114:251–262. <https://doi.org/10.1016/ISATRA.2020.12.029>
  61. Prashar N, Sood M, Jain S (2021) Design and implementation of a robust noise removal system in ECG signals using dual-tree complex wavelet transform. *Biomed Signal Process Control* 63:102212. <https://doi.org/10.1016/BSPC.2020.102212>
  62. Dotsinsky I, Christov I, Daskalov I (1996) Assessment of metrological characteristics of digital electrocardiographs. *J Clin Eng* 21(2):156
  63. García-Niebla J, Serra-Autonell G (2009) Effects of inadequate low-pass filter application. *J Electrocardiol* 42(4):303–304. <https://doi.org/10.1016/JELECTROCARD.2009.03.002>
  64. Mikiko N, Tsunemitsu C, Katoh S, Kamiyama Y, Sano N, Ezaki K, Miyazaki H et al (2014) Effect of ECG filter settings on J-waves. *J Electrocardiol* 47(1):7–11. <https://doi.org/10.1016/JELECTROCARD.2013.10.001>
  65. Christov I, Neycheva T, Schmid R, Stoyanov T, Abächerli R (2017) Pseudo-real-time low-pass filter in ECG, self-adjustable to the frequency spectra of the waves. *Med Biol Eng Compu* 55(9):1579–1588. <https://doi.org/10.1007/s11517-017-1625-y>
  66. Watford C (2014) Understanding ECG Filtering, EMS 12-Lead, EMS-Topics. <https://www.rigacci.org/wiki/lib/exe/fetch.php/tecnica/misc/ecg90a/understanding-ecg-filtering.pdf>. Accessed 11 Sept 2021
  67. Tantawi MM, Revett K, Salem A, Tolba MF (2013) Fiducial feature reduction analysis for electrocardiogram (ECG) based biometric recognition. *J Intell Inf Syst* 40(1):17–39. <https://doi.org/10.1007/s10844-012-0214-7>
  68. Coutinho DP, Silva H, Gamboa H, Fred A, Figueiredo M (2013) Novel fiducial and non-fiducial approaches to electrocardiogram-based biometric systems. *IET Biom* 2(2):64–75. <https://doi.org/10.1049/IET-BMT.2012.0055>
  69. Chua TW, Tan WW (2011) Non-singleton genetic fuzzy logic system for arrhythmias classification. *Eng Appl Artif Intell* 24(2):251–259. <https://doi.org/10.1016/ENGAPPAI.2010.10.003>
  70. Haseena HH, Mathew AT, Paul JK (2011) Fuzzy clustered probabilistic and multi layered feed forward neural networks for electrocardiogram arrhythmia classification. *J Med Syst* 35(2):179–188. <https://doi.org/10.1007/s10916-009-9355-9>
  71. Burguera A (2018) Fast QRS detection and ECG compression based on signal structural analysis. *IEEE J Biomed Health Inform* 23(1):123–131. <https://doi.org/10.1109/JBHI.2018.2792404>
  72. Vullings R, De Vries B, Bergmans JWM (2010) An adaptive Kalman filter for ECG signal enhancement. *IEEE Trans Biomed Eng* 58(4):1094–1103. <https://doi.org/10.1109/TBME.2010.2099229>
  73. Berkaya SK, Uysal AK, Gunal ES, Ergin S, Gunal S, Gulmezoglu MB (2018) A survey on ECG analysis. *Biomed Signal Process Control* 43:216–235. <https://doi.org/10.1016/BSPC.2018.03.003>
  74. Hiasat AA, Al-Ibrahim MM, Gharabeh KM (1999) Design and implementation of a new efficient median filtering algorithm. *IEE Proceedings-Vision, Image Signal Process* 146(5):273–278. <https://doi.org/10.1049/IP-VIS:19990444>
  75. Acharya D, Rani A, Agarwal S, Singh V (2016) Application of adaptive Savitzky-Golay filter for EEG signal processing. *Perspect Sci* 8:677–679. <https://doi.org/10.1016/PISC.2016.06.056>
  76. Widrow B, Glover JR, McCool JM, Kaunitz J, Williams CS, Hearn RH, Zeidler JR, Dong JRE, Goodlin RC (1975) Adaptive noise cancelling: principles and applications. *Proc IEEE* 63(12):1692–1716. <https://doi.org/10.1109/PROC.1975.10036>
  77. Thakor NV, Zhu Y-S (1991) Applications of adaptive filtering to ECG analysis: noise cancellation and arrhythmia detection. *IEEE Trans Biomed Eng* 38(8):785–794. <https://doi.org/10.1109/10.83591>
  78. Haykin SS (2008) Adaptive filter theory. Pearson Education India, Delhi
  79. Soria-Olivas E, Martinez-Sober M, Calpe-Maravilla J, Guerrero-Martinez JF, Chorro-Gascó J, Espí-López J (1998) Application of adaptive signal processing for determining the limits of P and T waves in an ECG. *IEEE Trans Biomed Eng* 45(8):1077–1080
  80. Smith SW (1997) The scientist and engineer's guide to digital signal processing. California Technical Publication, San Diego
  81. Li T, Wen P, Jayamaha S (2014) Anaesthetic EEG signal denoise using improved nonlocal mean methods. *Australas Phys Eng Sci Med* 37(2):431–437. <https://doi.org/10.1007/s13246-014-0263-z>
  82. Edmonson W, Palacios JC, Lai CA, Latchman H (1999) A global optimization method for continuous-time adaptive recursive filters. *IEEE Signal Process Lett* 6(8):199–201. <https://doi.org/10.1109/97.774864>

83. Sameni R, Shamsollahi MB, Jutten C, Clifford GD (2007) A nonlinear Bayesian filtering framework for ECG denoising. *IEEE Trans Biomed Eng* 54(12):2172–2185. <https://doi.org/10.1109/TBME.2007.897817>
84. Milchevski A, Gusev M (2016) Performance evaluation of FIR and IIR filtering of ECG signals. In: International conference on ICT innovations. Springer, Cham. pp. 103–112. [https://doi.org/10.1007/978-3-319-68855-8\\_10](https://doi.org/10.1007/978-3-319-68855-8_10)
85. Srivastva R, Singh YN (2019) ECG analysis for human recognition using non-fiducial methods. *IET Biom* 8(5):295–305. <https://doi.org/10.1049/IET-BMT.2018.5093>
86. Krishnan S, Athavale Y (2018) Trends in biomedical signal feature extraction. *Biomed Signal Process Control* 43:41–63. <https://doi.org/10.1016/BSPC.2018.02.008>
87. Pandya UT, Desai UB (2012) A novel algorithm for bluetooth ECG. *IEEE Trans Biomed Eng* 59(11):3148–3154. <https://doi.org/10.1109/TBME.2012.2217494>
88. Kumar A, Ranganatham R, Komaragiri R, Kumar M (2019) Efficient QRS complex detection algorithm based on Fast Fourier Transform. *Biomed Eng Lett* 9(1):145–151. <https://doi.org/10.1007/s13534-018-0087-y>
89. Noor SM, John E, Panday M (2018) Design and implementation of an ultralow-energy FFT ASIC for processing ECG in cardiac pacemakers. *IEEE Trans Very Large Scale Integr Syst* 27(4):983–987
90. Bendifallah A, Benzid R, Boulemden M (2011) Improved ECG compression method using discrete cosine transform. *Electron Lett* 47(2):87–89. <https://doi.org/10.1049/EL.2010.3191>
91. Benzid R, Messaoudi A, Boussaad A (2008) Constrained ECG compression algorithm using the block-based discrete cosine transform. *Dig Signal Process* 18(1):56–64. <https://doi.org/10.1016/DSP.2007.08.003>
92. Raj S, Ray KC (2017) ECG signal analysis using DCT-based DOST and PSO optimized SVM. *IEEE Trans Instrum Measurement* 66(3):470–478. <https://doi.org/10.1109/TIM.2016.2642758>
93. <https://cs.stanford.edu/people/eroberts/courses/soco/projects/data-compression/lossy/jpeg/dct.htm>. Accessed 7 May 2021
94. Shaik BS, Naganjaneyulu GVSSKR, Chandrasheker T, Narasimhadhan AV (2015) A method for QRS delineation based on STFT using adaptive threshold. *Proc Comput Sci* 54:646–653. <https://doi.org/10.1016/PROCS.2015.06.075>
95. Quatieri SNT, Lim J (1983) Signal reconstruction from short-time Fourier transform magnitude. *IEEE Trans Acoust, Speech, Signal Process* 31(4):986–998. <https://doi.org/10.1109/TASSP.1983.1164162>
96. Xie Q, Shikui Tu, Wang G, Lian Y, Lei Xu (2019) Feature enrichment based convolutional neural network for heartbeat classification from electrocardiogram. *IEEE Access* 7:153751–153760. <https://doi.org/10.1109/ACCESS.2019.2948857>
97. Singh BN, Tiwari AK (2006) Optimal selection of wavelet basis function applied to ECG signal denoising. *Digital Signal Process* 16(3):275–287. <https://doi.org/10.1016/DSP.2005.12.003>
98. Sabherwal P, Agrawal M, Singh L (2017) Automatic detection of the R peaks in single-lead ECG signal. *Circuits Syst Signal Process* 36(11):4637–4652. <https://doi.org/10.1007/s00034-017-0537-2>
99. Sahoo S, Biswal P, Das T, Sabut S (2016) De-noising of ECG signal and QRS detection using Hilbert transform and adaptive thresholding. *Proc Technol* 25:68–75. <https://doi.org/10.1016/PROTCY.2016.08.082>
100. Banerjee S, Gupta R, Mitra M (2012) Delineation of ECG characteristic features using multiresolution wavelet analysis method. *Measurement* 45(3):474–487. <https://doi.org/10.1016/MEASUREMENT.2011.10.025>
101. Rakshit M, Das S (2017) An efficient wavelet-based automated R-peaks detection method using Hilbert transform. *Biocybern Biomed Eng* 37(3):566–577. <https://doi.org/10.1016/BBE.2017.02.002>
102. Park J-S, Lee S-W, Park U (2017) R peak detection method using wavelet transform and modified Shannon energy envelope. *J Healthc Eng*. <https://doi.org/10.1155/2017/4901017>
103. Li C, Zheng C, Tai C (1995) Detection of ECG characteristic points using wavelet transforms. *IEEE Trans Biomed Eng* 42(1):21–28. <https://doi.org/10.1109/10.362922>
104. Li P, Zhang Xu, Liu M, Xiaohui Hu, Pang Bo, Yao Z, Jiang H, Chen H (2017) A 410-nW efficient QRS processor for mobile ECG monitoring in 0.18- $\mu$ m CMOS. *IEEE Trans Biomed Circuits Syst* 11(6):1356–1365. <https://doi.org/10.1109/TBCAS.2017.2731797>
105. Yochum M, Renaud C, Jacquir S (2016) Automatic detection of P, QRS and T patterns in 12 leads ECG signal based on CWT. *Biomed Signal Process Control*. <https://doi.org/10.1016/BSPC.2015.10.011>
106. Sabherwal P, Singh L, Agrawal M (2018) Aiding the detection of QRS complex in ECG signals by detecting S peaks independently. *Cardiovasc Eng Technol* 9(3):469–481. <https://doi.org/10.1007/s13239-018-0355-0>
107. Huang NE, Shen Z, Long SR, Wu MC, Shih EH, Zheng Q, Tung CC, Liu HH (1998) The empirical mode decomposition method and the Hilbert spectrum for non-stationary time series analysis. *Proc Roy Soc London* 454A:903–995. <https://doi.org/10.1098/RSPA.1998.0193>
108. Labate D, Foresta FL, Occhiuto G, Morabito FC, Lay-Ekuakille A, Vergallo P (2013) Empirical mode decomposition vs. wavelet decomposition for the extraction of respiratory signal from single-channel ECG: a comparison. *IEEE Sens J* 13(7):2666–2674. <https://doi.org/10.1109/JSEN.2013.2257742>
109. Karagiannis A, Constantinou P (2010) Noise-assisted data processing with empirical mode decomposition in biomedical signals. *IEEE Trans Inf Technol Biomed* 15(1):11–18. <https://doi.org/10.1109/TITB.2010.2091648>
110. Chang K-M (2010) Arrhythmia ECG noise reduction by ensemble empirical mode decomposition. *Sensors* 10(6):6063–6080. <https://doi.org/10.3390/s100606063>
111. Wu Z, Huang NE (2009) Ensemble empirical mode decomposition: a noise-assisted data analysis method. *Adv Adapt Data Anal* 1(01):1–41. <https://doi.org/10.1142/S1793536909000047>
112. Gaci S (2016) A new ensemble empirical mode decomposition (EEMD) denoising method for seismic signals. *Energy Proc* 97:84–91
113. Fosso, OB., Molinas M (2017) Method for mode mixing separation in empirical mode decomposition." *arXiv preprint*
114. Rajesh KNVPS, Dhuli R (2017) Classification of ECG heartbeats using nonlinear decomposition methods and support vector machine. *Comput Biol Med* 87:271–284. <https://doi.org/10.1016/COMPBIOMED.2017.06.006>
115. Jebaraj J, Arumugam R (2016) Ensemble empirical mode decomposition-based optimised power line interference removal algorithm for electrocardiogram signal. *IET Signal Proc* 10(6):583–591. <https://doi.org/10.1049/IET-SPR.2015.0292>
116. Maji U, Mitra M, Pal S (2015) Detection and characterisation of QRS complex in VMD domain pp. 101–5. <https://doi.org/10.1049/CP.2015.1697>
117. Goovaerts G, Padhy S, Vandenberk B, Varon C, Willems R, Huffel SV (2018) A machine-learning approach for detection and quantification of QRS fragmentation. *IEEE J Biomed Health Inform* 23(5):1980–1989. <https://doi.org/10.1109/JBHI.2018.2878492>
118. Gupta V, Mittal M, Mittal V (2019) R-peak detection using chaos analysis in standard and real time ECG databases. *IRBM* 40(6):341–354. <https://doi.org/10.1016/IRBM.2019.10.001>

119. Chawla MPS (2011) PCA and ICA processing methods for removal of artifacts and noise in electrocardiograms: a survey and comparison. *Appl Soft Comput* 11(2):2216–2226. <https://doi.org/10.1016/ASOC.2010.08.001>
120. Sharma T, Sharma KK (2017) QRS complex detection in ECG signals using locally adaptive weighted total variation denoising. *Comput Biol Med* 87:187–199. <https://doi.org/10.1016/COMPB.IOMED.2017.05.027>
121. Gutiérrez-Rivas R, García JJ, Marnane WP, Hernández A (2015) Novel real-time low-complexity QRS complex detector based on adaptive thresholding. *IEEE Sens J* 15(10):6036–6043. <https://doi.org/10.1109/JSEN.2015.2450773>
122. Christov II (2004) Real time electrocardiogram QRS detection using combined adaptive threshold. *Biomed Eng Online* 3(1):28. <https://doi.org/10.1186/1475-925X-3-28>
123. Castells-Rufas D, Carrabina J (2015) Simple real-time QRS detector with the MaMeMi filter. *Biomed Signal Process Control* 21:137–145. <https://doi.org/10.1016/BSPC.2015.06.001>
124. Rezik S, Ellouze N (2017) Enhanced and optimal algorithm for QRS detection. *Irbm* 38(1):56–61. <https://doi.org/10.1016/IRBM.2016.11.004>
125. Farashi S (2016) A multiresolution time-dependent entropy method for QRS complex detection. *Biomed Signal Process Control* 24:63–71. <https://doi.org/10.1016/BSPC.2015.09.008>
126. Hou Z, Dong Y, Xiang J, Li X, Yang B (2018) A real-time QRS detection method based on phase portraits and box-scoring calculation. *IEEE Sens J* 18(9):3694–3702. <https://doi.org/10.1109/JSEN.2018.2812792>
127. Modak S, Taha LY, Abdel-Raheem E (2021) A novel method of QRS detection using time and amplitude thresholds with statistical false peak elimination. *IEEE Access* 9:46079–46092. <https://doi.org/10.1109/ACCESS.2021.3067179>
128. Morshedlou F, Ravanshad N, Rezaee-Dehsorkh H (2021) An ultra-low power analog QRS-detection circuit for ambulatory ECG monitoring. *AEU-Int J Electron Commun* 129:153551. <https://doi.org/10.1016/AEUE.2020.153551>
129. Kumar A, Ranganatham R, Singh S, Komaragiri R, Kumar M (2021) A robust digital ECG signal watermarking and compression using biorthogonal wavelet transform. *Res Biomed Eng* 37(1):79–85. <https://doi.org/10.1007/s42600-020-00108-1>
130. Kumar A, Komaragiri R, Kumar M (2018) From pacemaker to wearable: techniques for ECG detection systems. *J Med Syst* 42(2):1–17. <https://doi.org/10.1007/s10916-017-0886-1>
131. Kumar A, Kumar M, Komaragiri R (2018) Design of a biorthogonal wavelet transform based R-peak detection and data compression scheme for implantable cardiac pacemaker systems. *J Med Syst* 42(6):1–12. <https://doi.org/10.1007/s10916-018-0953-2>
132. Kumar A, Mehla VK, Tomar H, Kumar M, Komaragiri R (2020) Classification of normal and abnormal ECG signals using support vector machine and Fourier decomposition method. In: 2020 IEEE International symposium on smart electronic systems (iSES)(Formerly iNiS), pp. 161–166. IEEE, 2020. <https://doi.org/10.1109/iSES50453.2020.00044>
133. Saadi DB, Tanev G, Flintrup M, Osmanagic A, Egstrup K, Hoppe K, Jennum P, Jeppesen JL, Iversen HK, Sorensen HBD (2015) Automatic real-time embedded QRS complex detection for a novel patch-type electrocardiogram recorder. *IEEE J Transl Eng Health Med* 3:1–12. <https://doi.org/10.1109/JTEHM.2015.2421901>
134. Kim J, Shin H (2016) Simple and robust realtime QRS detection algorithm based on spatiotemporal characteristic of the QRS complex. *PLoS ONE* 11(3):e0150144. <https://doi.org/10.1371/JOURNAL.PONE.0150144>
135. Yakut Ö, Bolat ED (2018) An improved QRS complex detection method having low computational load. *Biomed Signal Process Control* 42:230–241. <https://doi.org/10.1016/BSPC.2018.02.004>
136. Ferdi Y, Herbeuval JP, Charef A, Boucheham B (2003) R wave detection using fractional digital differentiation. *ITBM-RBM* 24(5–6):273–280. <https://doi.org/10.1016/RBMRET.2003.08.002>
137. Benmalek M, Charef A (2009) Digital fractional order operators for R-wave detection in electrocardiogram signal. *IET Signal Proc* 3(5):381–391. <https://doi.org/10.1049/IET-SPR.2008.0094>
138. Nayak C, Saha SK, Kar R, Mandal D (2018) Automated QRS complex detection using MFO-based DFOD. *IET Signal Process* 12(9):1172–1184. <https://doi.org/10.1049/IET-SPR.2018.5230>
139. Nayak C, Saha SK, Kar R, Mandal D (2019) An efficient QRS complex detection using optimally designed digital differentiator. *Circuits, Syst, Signal Process* 38(2):716–749. <https://doi.org/10.1007/s00034-018-0880-y>
140. Bashar SK, Noh Y, Walkey AJ, McManus DD, Chon KH (2019) VERB: VFCDM-based electrocardiogram reconstruction and beat detection algorithm. *IEEE Access* 7:13856–13866
141. Chin W-L, Chang C-C, Tseng C-L, Huang Y-Z, Jiang T (2019) Bayesian real-time QRS complex detector for healthcare system. *IEEE Internet Things J* 6(3):5540–5549. <https://doi.org/10.1109/JIOT.2019.2903530>
142. Nayak C, Saha SK, Kar R, Mandal D (2019) An efficient and robust digital fractional order differentiator-based ECG Pre-processor design for QRS detection. *IEEE Trans Biomed Circuits Syst* 13(4):682–696. <https://doi.org/10.1109/TBCAS.2019.2916676>
143. Nayak C, Saha SK, Kar R, Mandal D (2019) An optimally designed digital differentiator based preprocessor for R-peak detection in electrocardiogram signal. *Biomed Signal Process Control* 49:440–464. <https://doi.org/10.1016/BSPC.2018.09.005>
144. Yazdani S, Vesin J-M (2016) Extraction of QRS fiducial points from the ECG using adaptive mathematical morphology. *Dig Signal Process* 56:100–109. <https://doi.org/10.1016/DSP.2016.06.010>
145. Jain S, Kumar A, Bajaj V (2016) Technique for QRS complex detection using particle swarm optimisation. *IET Signal Proc* 10(6):626–636. <https://doi.org/10.1049/IET-SMT.2016.0023>
146. Pandit D, Zhang L, Liu C, Chattopadhyay S, Aslam N, Lim CP (2017) A lightweight QRS detector for single lead ECG signals using a max-min difference algorithm. *Comput Methods Prog Biomed* 144:61–75. <https://doi.org/10.1016/CMPB.2017.02.028>
147. Lee M, Park D, Dong S-Y, Youn I (2018) A novel R peak detection method for mobile environments. *IEEE Access* 6:51227–51237. <https://doi.org/10.1109/ACCESS.2018.2867329>
148. Sharma LD, Sunkaria RK (2016) A robust QRS detection using novel pre-processing techniques and kurtosis based enhanced efficiency. *Measurement* 87:194–204. <https://doi.org/10.1016/MEASUREMENT.2016.03.015>
149. Jain S, Ahirwal MK, Kumar A, Bajaj V, Singh GK (2017) QRS detection using adaptive filters: a comparative study. *ISA Trans* 66:362–375. <https://doi.org/10.1016/ISATRA.2016.09.023>
150. Elgendi M, Mohamed A, Ward R (2017) Efficient ECG compression and QRS detection for e-health applications. *Sci Rep* 7(1):1–16. <https://doi.org/10.1038/s41598-017-00540-x>
151. Zidelmal Z, Amirou A, Ould-Abdeslam D, Moukadem A, Dietlerlen A (2014) QRS detection using S-Transform and Shannon energy. *Comput Methods Prog Biomed* 116(1):1–9. <https://doi.org/10.1016/CMPB.2014.04.008>
152. Biswal B (2017) ECG signal analysis using modified S-transform. *Healthc Technol Lett* 4(2):68–72. <https://doi.org/10.1049/HTL.2016.0078>
153. Chen C-L, Chuang C-T (2017) A QRS detection and R point recognition method for wearable single-lead ECG devices. *Sensors* 17(9):1969. <https://doi.org/10.3390/s17091969>

154. Merah M, Abdelmalik TA, Larbi BH (2015) R-peaks detection based on stationary wavelet transform. *Comput Methods Progr Biomed* 121(3):149–160. <https://doi.org/10.1016/CMPB.2015.06.003>
155. Berwal D, Kumar A, Kumar Y (2018) Design of high performance QRS complex detector for wearable healthcare devices using biorthogonal spline wavelet transform. *ISA Trans* 81:222–230. <https://doi.org/10.1016/ISATRA.2018.08.002>
156. Sharma A, Patidar S, Upadhyay A, Acharya UR (2019) Accurate tunable-Q wavelet transform based method for QRS complex detection. *Comput Electr Eng* 75:101–111. <https://doi.org/10.1016/COMPELECENG.2019.01.025>
157. Ravanshad N, Rezaee-Dehsorkh H, Lotfi R, Lian Y (2013) A level-crossing based QRS-detection algorithm for wearable ECG sensors. *IEEE J Biomed Health Inform* 18(1):183–192. <https://doi.org/10.1109/JBHI.2013.2274809>
158. Qin Q, Li J, Yue Y, Liu C (2017) An adaptive and time-efficient ECG R-peak detection algorithm. *J Healthc Eng*. <https://doi.org/10.1155/2017/5980541>
159. Deepu CJ, Lian Y (2014) A joint QRS detection and data compression scheme for wearable sensors. *IEEE Trans Biomed Eng* 62(1):165–175. <https://doi.org/10.1109/TBME.2014.2342879>
160. Tang X, Qisong Hu, Tang W (2018) A real-time QRS detection system with PR/RT interval and ST segment measurements for wearable ECG sensors using parallel delta modulators. *IEEE Trans Biomed Circuits Syst* 12(4):751–761. <https://doi.org/10.1109/TBCAS.2018.2823275>
161. Li Y, Tang X, Zhi Xu, Yan H (2018) A novel approach to phase space reconstruction of single lead ECG for QRS complex detection. *Biomed Signal Process Control* 39:405–415. <https://doi.org/10.1016/BSPC.2017.06.007>
162. Bajaj A, Kumar S (2019) QRS complex detection using fractional Stockwell transform and fractional Stockwell Shannon energy. *Biomed Signal Process Control* 54:101628. <https://doi.org/10.1016/BSPC.2019.101628>
163. Hossain MB, Bashar SK, Walkey AJ, McManus DD, Chon KH (2019) An accurate QRS complex and P-wave detection in ECG signals using complete ensemble empirical mode decomposition with adaptive noise approach. *IEEE Access* 7:128869–128880. <https://doi.org/10.1109/ACCESS.2019.2939943>
164. Jia M, Li F, Jiaquan Wu, Chen Z, Yu Pu (2020) Robust QRS detection using high-resolution wavelet packet decomposition and time-attention convolutional neural network. *IEEE Access* 8:16979–16988. <https://doi.org/10.1109/ACCESS.2020.2967775>
165. Chen H, Maharatna K (2020) An automatic R and T peak detection method based on the combination of hierarchical clustering and discrete wavelet transform. *IEEE J Biomed Health Inform* 24(10):2825–2832. <https://doi.org/10.1109/JBHI.2020.2973982>
166. Fotoohinasab A, Hocking T, Afghah F (2021) A greedy graph search algorithm based on changepoint analysis for automatic QRS complex detection. *Comput Biol Med* 130:104208. <https://doi.org/10.1016/COMPBIOMED.2021.104208>
167. Coast DA, Stern RM, Cano GG, Brillier SA (1990) An approach to cardiac arrhythmia analysis using hidden Markov models. *IEEE Trans Biomed Eng* 37(9):826–836. <https://doi.org/10.1109/10.58593>
168. Kohler B-U, Hennig C, Orglmeister R (2002) The principles of software QRS detection. *IEEE Eng Med Biol Mag* 21(1):42–57. <https://doi.org/10.1109/51.993193>
169. Silipo R, Marchesi C (1998) Artificial neural networks for automatic ECG analysis. *IEEE Trans Signal Process* 46(5):1417–1425. <https://doi.org/10.1109/78.668803>
170. Kohler BU, Hennig C, Orglmeister R (2003) QRS detection using zero crossing counts. *Appl Genomics Proteomics* 2(2):138–145
171. Nyquist H (1928) Certain topics in telegraph transmission theory. *Trans Am Inst Electr Eng* 47(2):617–644. <https://doi.org/10.1109/T-AIEE.1928.5055024>
172. Ajaraga E, Gusev M (2017) Analysis of sampling frequency and resolution in ECG signals. In: 2017 25th Telecommunication Forum (TELFOR), pp. 1–4. IEEE. <https://doi.org/10.1109/TELFOR.2017.8249438>
173. Bailey JJ, Berson AS, Garson A Jr, Horan LG, Macfarlane PW, Mortara DW, Zywiec C (1990) Recommendations for standardization and specifications in automated electrocardiography: bandwidth and digital signal processing. A report for health professionals by an ad hoc writing group of the committee on electrocardiography and cardiac electrophysiology of the council on clinical cardiology, American heart association. *Circulation* 81(2):730–739
174. Malik M (1996) Task force of the European society of cardiology and the North American society of pacing and electrophysiology. Heart rate variability. Standards of measurement, physiological interpretation, and clinical use. *Eur Heart J* 17:354–381
175. Goldberger AL, Amaral LAN, Glass L, Hausdorff JM, Ivanov PC, Mark RG, Mietus JE, Moody GB, Peng CK, Stanley HE (2000) PhysioBank, physiotoolkit, and physionet—components of a new research resource for complex physiologic signals. *Circulation* 101:E215–E220
176. Amann A, Tratnig R, Unterkofler K (2006) Detecting ventricular fibrillation by time-delay methods. *IEEE Trans Biomed Eng* 54(1):174–177. <https://doi.org/10.1109/TBME.2006.880909>
177. Amann A, Tratnig R, Unterkofler K (2005) Reliability of old and new ventricular fibrillation detection algorithms for automated external defibrillators. *Biomed Eng Online* 4(1):60. <https://doi.org/10.1186/1475-925X-4-60>
178. American Heart Association (1989) AHA database. URL <https://www.americanheart.org>
179. Nolle FM, Badura FK, Catlett JM, Bowser RW, Sketch MH (1986) CREI-GARD, a new concept in computerized arrhythmia monitoring systems. *Comput Cardiol* 13:515–518
180. Laguna P, Mark RG, Goldberg A, Moody GB (1997) A database for evaluation of algorithms for measurement of QT and other waveform intervals in the ECG. In: *Computers in Cardiology, IEEE*. <https://doi.org/10.1109/CIC.1997.648140>
181. Behar JA, Bonnemains L, Shulgin V, Oster J, Ostrass O, Lakhno I (2019) Noninvasive fetal electrocardiography for the detection of fetal arrhythmias. *Prenat Diagn* 39(3):178–187. <https://doi.org/10.1002/PD.5412>
182. Penzel T, Moody GB, Mark RG, Goldberger AL, Peter JH (2000) The apnea-ECG database. In: *Computers in cardiology 2000*. Vol. 27 (Cat. 00CH37163), pp. 255–258. IEEE, <https://doi.org/10.1109/CIC.2000.898505>
183. Andreotti F, Behar J, Zaunseder S, Oster J, Clifford GD (2016) An open-source framework for stress-testing non-invasive fetal ECG extraction algorithms. *Physiol Meas* 37(5):627
184. Iyengar N, Peng CK, Morin R, Goldberger AL, Lipsitz LA (1996) Age-related alterations in the fractal scaling of cardiac interbeat interval dynamics. *Am J Physiology-Regulatory, Integr Comp Physiol* 271(4):R1078–R1084. <https://doi.org/10.1152/AJPRE GU.1996.271.4.R1078>
185. Baim DS, Colucci WS, Scott Monrad E, Smith HS, Wright RF, Lanoue A, Gauthier DF, Ransil BJ, Grossman W, Braunwald E (1986) Survival of patients with severe congestive heart failure treated with oral milrinone. *J Am Coll Cardiol* 7(3):661–670. [https://doi.org/10.1016/S0735-1097\(86\)80478-8](https://doi.org/10.1016/S0735-1097(86)80478-8)
186. Albrecht P (1983) ST segment characterization for long term automated ECG analysis. PhD diss., Massachusetts Institute of Technology, Department of Electrical Engineering and Computer Science

187. Moody GB, Mark RG (2001) The impact of the MIT-BIH arrhythmia database. *IEEE Eng Med Biol Mag* 20(3):45–50. <https://doi.org/10.1109/51.932724>
188. Moody G (1983) A new method for detecting atrial fibrillation using RR intervals. *Comput Cardiol* 227–230
189. Taddei A, Distanti G, Emdin M, Pisani P, Moody GB, Zeelenberg C, Marchesi C (1992) The European ST-T database: standard for evaluating systems for the analysis of ST-T changes in ambulatory electrocardiography. *Eur Heart J* 13(9):1164–1172. <https://doi.org/10.1093/oxfordjournals.eurheartj.a060332>
190. Bousseljot R, Kreiseler D, Schnabel A (1995) Nutzung der EKG-Signaldatenbank CARDIODAT der PTB über das Internet. *Biomedizinische Technik/Biomed Eng* 40(s1):317–318. <https://doi.org/10.1515/BMTE.1995.40.s1.317>

**Publisher's Note** Springer Nature remains neutral with regard to jurisdictional claims in published maps and institutional affiliations.